5. Results and discussions

5.1. HPLC analytical method development

The method was developed on Waters HPLC having photodiode array detector. The separation was achieved by using C18 spherisorb 5.0 µm ODS2 4.6 mm x 250 mm column. In method development a series of mobile phase consisting of acetonitrile, methanol, water and buffer (pH range 2.5 to 8.0) were tried and further mobile phase was selected on peak parameters (symmetry, tailing), run time, ease of preparation and cost. Finally, the mobile phase consisted of acetonitrile and phosphate buffer (pH 3.3) in the ratio of 75:25 and at a flow rate of 1.0 ml/min. All the prepared solutions were represented as equivalent of asenapine concentration. For validation process paliperidone was used as internal standard. The peak shape and symmetry of internal standard were found to be good at proposed mobile composition and there were no interference with drug peak.

5.1.1. Method validation

System suitability

Three replicate of ASN solution and internal standard was injected and % relative standard deviation of peak area and retention time measured and it was within 2% indicating the suitability of system (Table 5.1).

Table 5.1: System suitability study

	Asenapine (10 µg/ml)		Internal standard (10 µg/ml)	
	Retention time (min)	**Peak area**	**Retention time (min)**	**Peak area**
Mean (n=3)	4.072	83072	3.2	54275
SD	0.057	652.2	0.026	873.8
%RSD	1.398	0.785	0.812	1.609

Linearity

The linearity was evaluated by linear regression analysis that was calculated by the least square regression method. It was determined over the six concentration range from 10-100 µg/ml. The peak area ratio of the drug to the IS was considered for the plotting the linearity graph. The equation for the resultant calibration curve was y=0.0609X+0.1024 and a linear regression coefficient was found to be 0.9988. Results obtained from regression analysis of the linearity data for asenapine is summarized in Table 5.2.

Table 5.2: Results of regression analysis of linearity data of asenapine

Parameters	Results
Range (µg/ml)	10.0–100.0
Regression equation	y=0.0609X+0.1024
R^2	0.9988
LOD (µg/ml)	1.0
LOQ (µg/ml)	5.0

Accuracy and Precision

Accuracy and precision were calculated for the QC samples and results are shown in Table 5.3 and 5.4, respectively. In accuracy test, each solutions was injected (n=3) and the percentage recovery was determined. The method shows a high percentage recovery for all solutions tested. The intra assay precision was found to be less than 1.62% RSD for all samples in all days. Inter-day precision % RSD for analysis conducted on three separate days was found to be 1.73, 0.13 and 0.71% RSD for low, medium and high concentration studies, respectively.

Table 5.3: Accuracy and percent bias

Concentration (µg/ml)	Determined concentration (µg/ml)	%Recovery
10	10.04	100.4
40	39.56	98.90
80	80.9	101.12

Table 5.4: Intra and inter day precision

Concentration (µg/ml)	Day 1		Day 2		Day 3		Intermediate precision
	Mean conc. (µg/ml)	%RSD	Mean conc. (µg/ml)	%RSD	Mean conc. (µg/ml)	%RSD	%RSD
10	9.74	1.44	9.88	1.62	10.08	1.19	1.73
40	40.14	1.32	40.21	1.47	40.24	1.04	0.13
80	79.72	1.10	80.87	1.01	80.21	1.15	0.71

Limit of detection and quantitation (Sensitivity)

The LOD for a signal to noise ratio of 3:1 was found to be 1.0 µg/ml (RSD ± 0.086%) whereas LOQ for a signal to noise ratio of 10:1 was 5.0 µg/ml (RSD ± 0.075%). These results indicated the sensitivity of the method was adequate (Table 5.2).

Robustness

The standard deviation of retention time and peak areas were calculated for each set of conditions and found to be <2%. The low values of RSD obtained after introduction of small deliberate changes in the conditions indicate the method is robust (Table 5.5).

Table 5.5: Robustness of method

Variable parameter	Retention time (%value ± SD, %RSD)	Peak area (%value ± SD, %RSD)
Flow rate (0.8-1.2 ml/min)	100.13±1.23, 1.14	100.02±1.45, 1.44
Mobile phase composition (± 2%)	99.45±1.42, 1.42	99.65±1.34, 1.34
pH (±0.05%)	100.12±1.62, 1.61	100.15±1.36, 1.35

5.1.2. Application of method

The developed method was applied for the determination of asenapine in pharmaceutical dosage form as well as drug lipid matrix. The assay result gave yield value 98.92- 99.52% of claim amount for the tested samples. No interference of excipients was observed with peak of drug. The spectrum of asenapine extracted from the sample was matching with that of standard asenapine chromatogram. The

results of the assay indicated that the method is selective for the assay of asenapine without interference from the excipients used in dosage forms. The representative chromatographs of concentration 10-100 µg/ml were presented in Figure 5.1 (a-f).

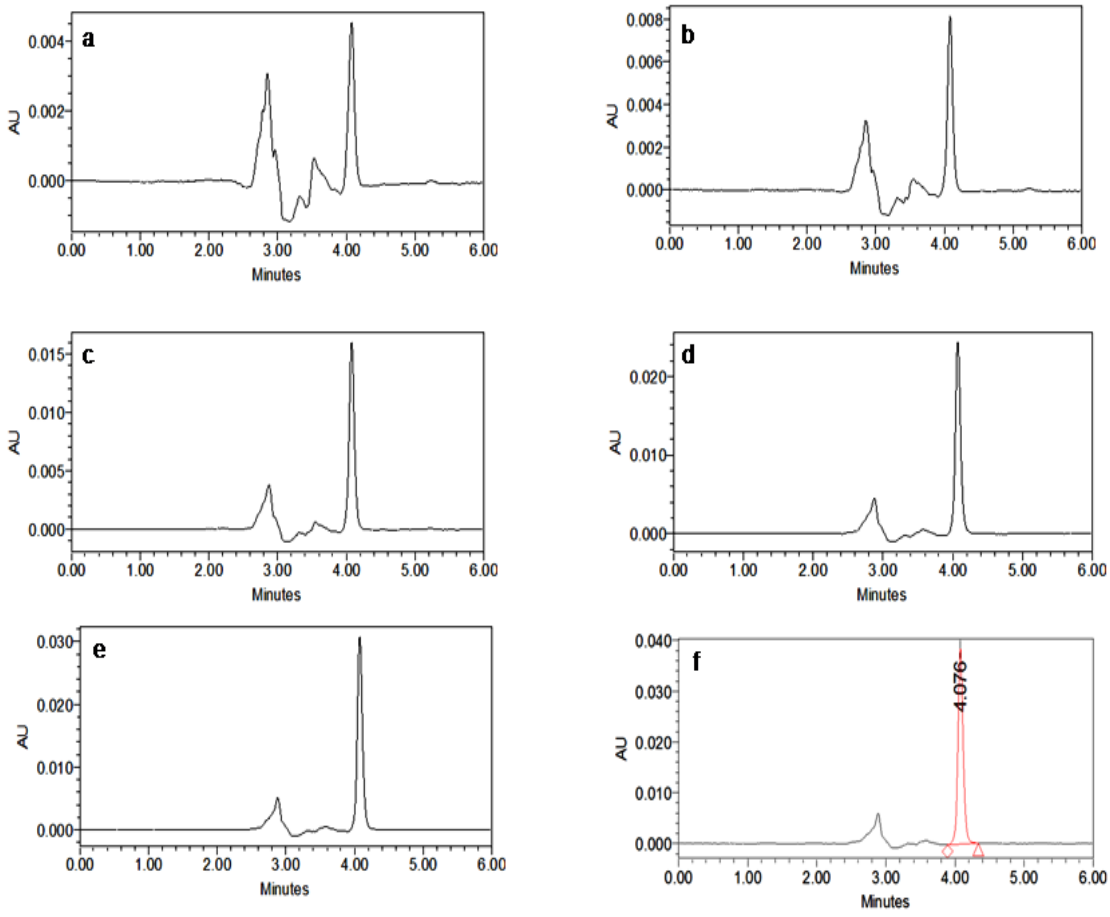

Figure 5.1: HPLC chromatograph of concentration (a) 10 µg/ml, (b) 20 µg/ml, (c) 40 µg/ml, (d) 60 µg/ml, (e) 80 µg/ml and (f) 100 µg/ml

The developed RP-HPLC method for quantitative determination of asenapine was found to be sensitive, precise, accurate specific and stability indicating. This developed method has been validated as per regulatory requirements. In this study, the use of C18 column and a simple mobile phase composition indicates that method

is suitable for routine quantitative analysis of asenapine in bulk and pharmaceutical dosage form. The rapid run time of 6 min allows the analysis of large number of samples with less mobile phase that proves to be cost-effective.

5.2. Optimization of NLC and statistical analysis of variables

A total of 46 experimental runs were generated from five factors, three levels box-behnken statistical experimental design with six centre point. The values of responses (dependent variables) are given in Table 5.6. The polynomial equations were generated for each response which explained the main effects, interaction effects and quadratic effect of independent variables. The smaller value of PRESS statistic and non significant lack of fit indicates the better model towards data points. A three-dimensional response surface plot was used to study interaction effects of independent variables on the response. A mathematical equation was generated for each response to evaluate the effect of factors. In this equation, a positive and negative value of independent factor represents direct and indirect effect on response (Chopra S *et al.*, 2007; Mujtaba A *et al.*, 2014).

The preliminary diagnostic study for entrapment efficiency revealed the anomalous response of batch NLC 22. It might be an experimental error. Indeed, this batch was excluded from further statistical analysis and batch optimization. The analysis of lack of fit and model fit summary revealed significant lack of fit for polydispersity index response in all studies model. So, this response was not considered for optimization of formulation. Further, only particle size and entrapment efficiency were selected for optimization and their respective lack of fit and model fit

summary is presented in Table 5.7. This table showed that the best-fitted model for dependent variable was quadratic. The non-significant model term was removed from analysis and it was not consider for generation of polynomial response equation of particle size and entrapment efficiency.

Table 5.6: Composition of different batches and their response (Mean±SD)

Batch No	Results (Response)		
	Particle Size (nm)	Entrapment efficiency (%)	Polydispersity index
NLC -1	274.65±4.51	75.72±1.83	0.293±0.015
NLC -2	309.75±3.63	69.62±2.52	0.361±0.027
NLC -3	275.63±5.46	74.83±1.58	0.293±0.023
NLC -4	195.51±6.35	59.93±2.62	0.220±0.018
NLC -5	298.46±2.23	67.19±3.23	0.415±0.038
NLC -6	310.98±.3.71	87.22±1.71	0.373±0.022
NLC -7	334.61±4.89	89.78±2.34	0.393±0.027
NLC -8	275.61±2.35	74.14±2.61	0.296±0.011
NLC -9	250.39±2.34	77.56±3.27	0.333±0.029
NLC -10	297.27±5.25	69.72±1.54	0.293±0.021
NLC -11	195.33±6.38	52.64±1.35	0.196±0.012
NLC -12	245.51±4.63	69.26±2.42	0.250±0.023
NLC -13	278.39±2.36	76.16±2.31	0.295±0.018
NLC -14	274.52±2.02	91.94±2.12	0.257±0.017
NLC -15	316.24±5.62	88.16±2.62	0.396±0.026
NLC -16	215.21±4.66	60.35±1.14	0.248±0.021
NLC -17	305.14±7.63	92.56±1.65	0.255±0.024
NLC -18	230.15±6.42	76.78±2.57	0.303±0.014
NLC -19	223.62±5.72	69.71±2.67	0.277±0.026

NLC -20	165.62±6.36	59.74±3.60	0.237±0.012
NLC -21	262.32±4.68	52.42±2.46	0.310±0.028
NLC -22	211.35±7.56	74.97±3.25	0.271±0.022
NLC -23	277.34±8.34	74.26±2.61	0.295±0.013
NLC -24	275.62±7.35	70.62±2.52	0.290±0.024
NLC -25	291.25±7.25	92.27±1.75	0.306±0.031
NLC -26	245.36±4.40	76.24±2.74	0.275±0.023
NLC -27	198.53±3.83	86.18±2.96	0.184±0.013
NLC -28	331.32±2.52	91.36±1.71	0.374±0.032
NLC -29	284.21±3.61	75.82±4.38	0.343±0.012
NLC -30	265.76±7.34	77.93±2.23	0.305±0.022
NLC -31	273.46±6.32	72.61±3.21	0.297±0.021
NLC -32	251.25±9.46	87.13±3.67	0.203±0.024
NLC -33	224.97±6.30	62.28±2.36	0.252±0.025
NLC -34	325.63±4.75	87.86±3.83	0.345±0.032
NLC -35	288.26±4.72	94.36±1.32	0.282±0.032
NLC -36	280.45±9.43	77.15±4.86	0.317±0.031
NLC -37	210.15±5.27	51.72±3.98	0.294±0.026
NLC -38	290.52±8.21	62.78±4.92	0.368±0.014
NLC -39	236.26±3.67	67.37±2.71	0.301±0.030
NLC -40	226.86±4.44	86.62±3.72	0.213±0.021
NLC -41	147.78±2.35	51.28±4.22	0.182±0.012
NLC -42	230.24±3.56	51.23±3.14	0.324±0.019
NLC -43	165.26±2.46	52.67±2.84	0.211±0.015
NLC -44	201.62±4.72	79.16±2.92	0.163±0.012
NLC -45	322.62±3.47	89.45±3.17	0.423±0.038
NLC -46	253.25±3.78	75.26±2.29	0.353±0.033

Table 5.7: Statistical analysis results of lack of fit test and model summary for particle size and entrapment efficiency

Model	Lack of fit tests					Model summary statistics					Remark
	SS	df	MS	F-value	p-value Prob>F	SD	R^2	Adjusted R^2	Predicted R^2	PRESS	
Particle Size											
Linear	10991.06	34	323.27	101.47	<0.0001	16.80	0.8839	0.8690	0.8462	14580.54	
2FI	10889.56	24	453.73	142.42	<0.0001	19.39	0.8849	0.8254	0.7136	27146.81	
Quadratic	50.02	19	2.63	0.83	0.6578	1.66	0.9993	0.9987	0.9975	232.59	Suggested
Cubic	14.02	4	3.50	1.10	0.4478	1.82	0.9997	0.9985	-	+	Aliased
Pure error	15.93	5	3.19	-	-	-	-	-	-	-	
Entrapment Efficiency											
Linear	282.71	34	8.32	5.18	0.0369	2.73	0.9601	0.9550	0.9453	398.05	
2FI	189.14	24	7.88	4.91	0.0423	2.61	0.9729	0.9589	0.9269	532.26	
Quadratic	55.84	19	2.94	1.83	0.2608	1.63	0.9912	0.9839	0.9664	244.65	Suggested
Cubic	0.28	4	0.070	0.043	0.9953	0.96	0.9989	0.9944	-	+	Aliased
Pure error	8.03	5	1.61	-	-	-	-	-	-	-	

SS: Sum of Squares, df: Degree of freedom, MS: Mean square, SD: Standard deviation, PRESS: Predicted Residual Error Sum of Squares; 2FI: Two factor interaction, + : PRESS statistic not defined, P-value <0.05 was considered as statistically significant.

5.2.1. Effect on particle size

The particle size (PS) of the prepared batches was in range of 147.78 - 334.61 nm. The quadratic model was selected for the analysis of variables on particles size based on the lack of fit test and model summary statistics. ANOVA for response surface quadratic model showed that A, B, C, D, E, AD, A^2, B^2, C^2, D^2 and E^2 were significant model terms. The final mathematical model in terms of coded factors determined by Design-Expert software is shown below:

PS = +275.85 -4.54 A +25.20 B -45.01 C -29.34 D -42.71 E +3.16 AD -4.57 A^2 +10.05 B^2 -20.73 C^2 -15.64 D^2 -21.90 E^2

Lower value of PRESS (232.59) and non significant lack of fit (F-value = 0.83, and p value = 0.6578) for quadratic model suggested that this model is fit to describe the effect of independent variables on particle size. Except ASM/GMS ratio (B), which have positive coefficient, all others model terms have negative coefficients. This suggested that particle size increases with increase in ASM/GMS ratio (B). Also, higher coefficient value (45.01) of surfactant concentration (C) suggested it had most significant effect on the particle size followed by E, D, B and A. It shows that stabilization effect of surfactant is critical factor for the preparation of NLC. While in case of the interaction effects between different factors, only OA/GMS ratio (A) and homogenization speed (D) had combined significant effect on particle size. It was visually discerned from 2D and 3D response surface plots in Figure 5.2.

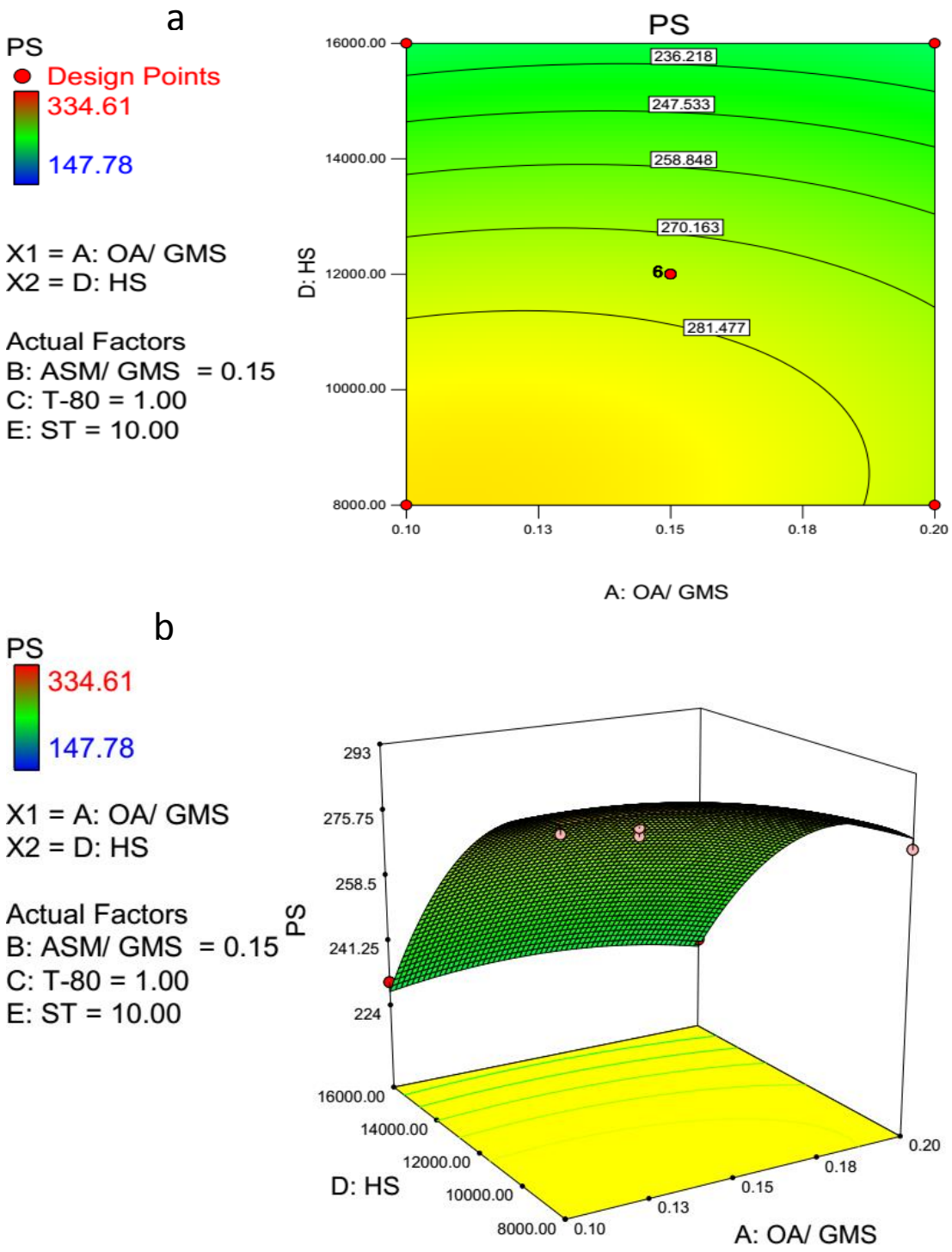

Figure 5.2: 2D (a) and 3D (b) graphical illustrations representing the interaction effect of drug/solid lipid ratio to homogenization on particle size

5.2.2. Effect on entrapment efficiency

The entrapment efficiency (EE) was in between the 51.23% to 92.56% in developed batches. The lack of fit test and model summary statistics elucidated higher adjusted (0.9839) and predicted (0.9664) R^2 values for quadratic model. Thus this model was selected for analysis of independent variables on entrapment efficiency. From the ANOVA, only terms A, B, C, D, E, AB, AC, AE, D^2 and E^2 were significant. The final mathematical equation with significant model term in coded factors is shown below:

EE = + 74.62 + 15.31 A + 7.41 B - 7.11 C - 4.95 D - 11.78 E - 2.94 AB + 2.35AC + 3.50 AE - 1.35 D^2 - 3.28 E^2

Lower value of PRESS (244.65) and non significant lack of fit (F-value = 1.83, and p value = 0.2608) for quadratic model suggested that this model fit to describe the effect of independent variables on entrapment efficiency. There was increase in entrapment efficiently with increase in the model term A and B. This indicates that higher concentration of liquid lipid and drug is favorable for higher entrapment efficiency. This could be justified by the higher solubility of drug in liquid lipid as compared to solid lipid in selected drug/lipid ratios. Moreover, the surfactant concentration (C), homogenization speed (D) and sonication time (E) have negative coefficient indicating that EE is inversely proportional to these factors. Here, the interaction term AB, AC and AE had the significant effect on the EE and it has been shown in Figure 5.3 to Figure 5.5 as 2D and 3D response surface plot.

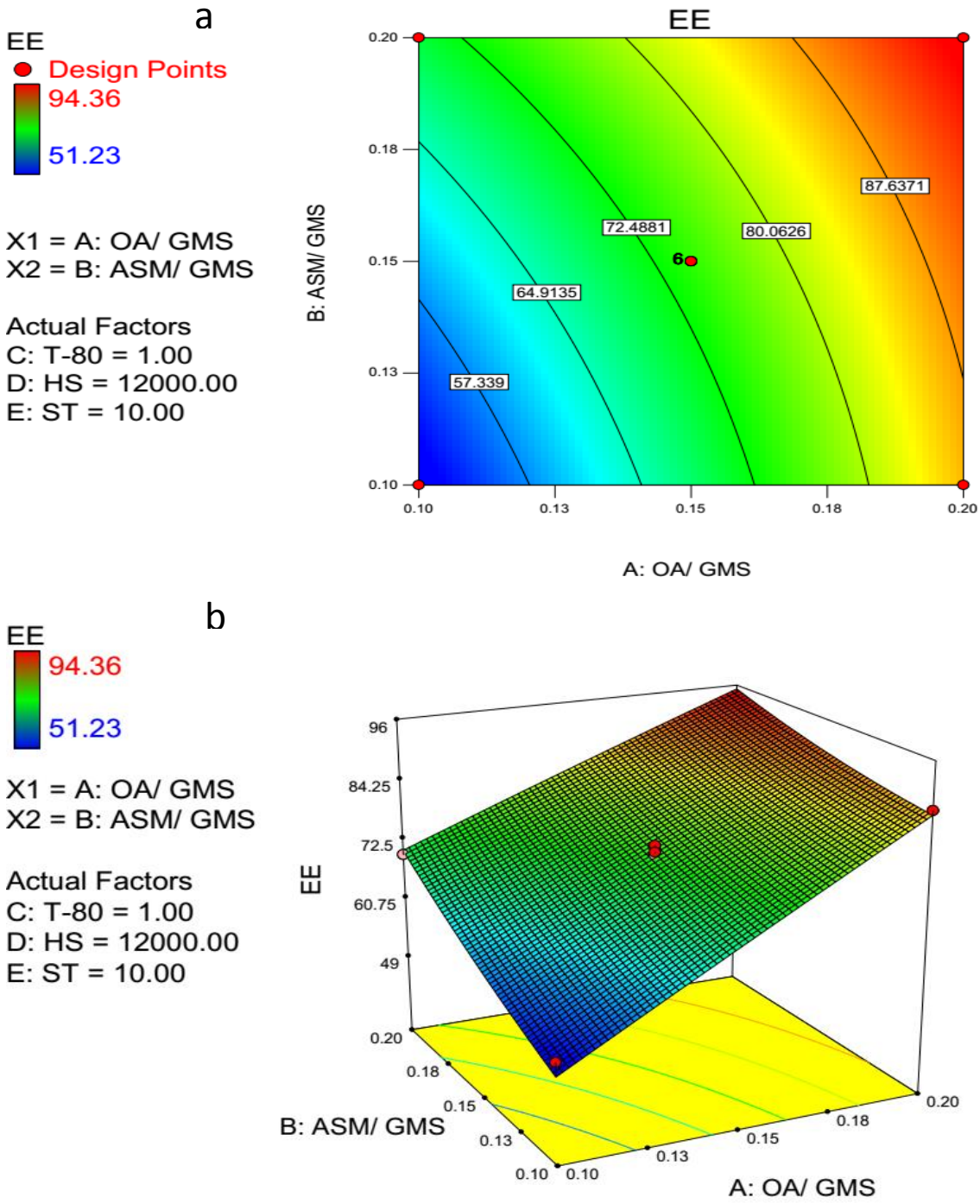

Figure 5.3: 2D (a) and 3D (b) graphical illustrations representing the interaction effect of liquid/solid lipid ratio to drug/solid lipid ratio on entrapment efficiency (EE)

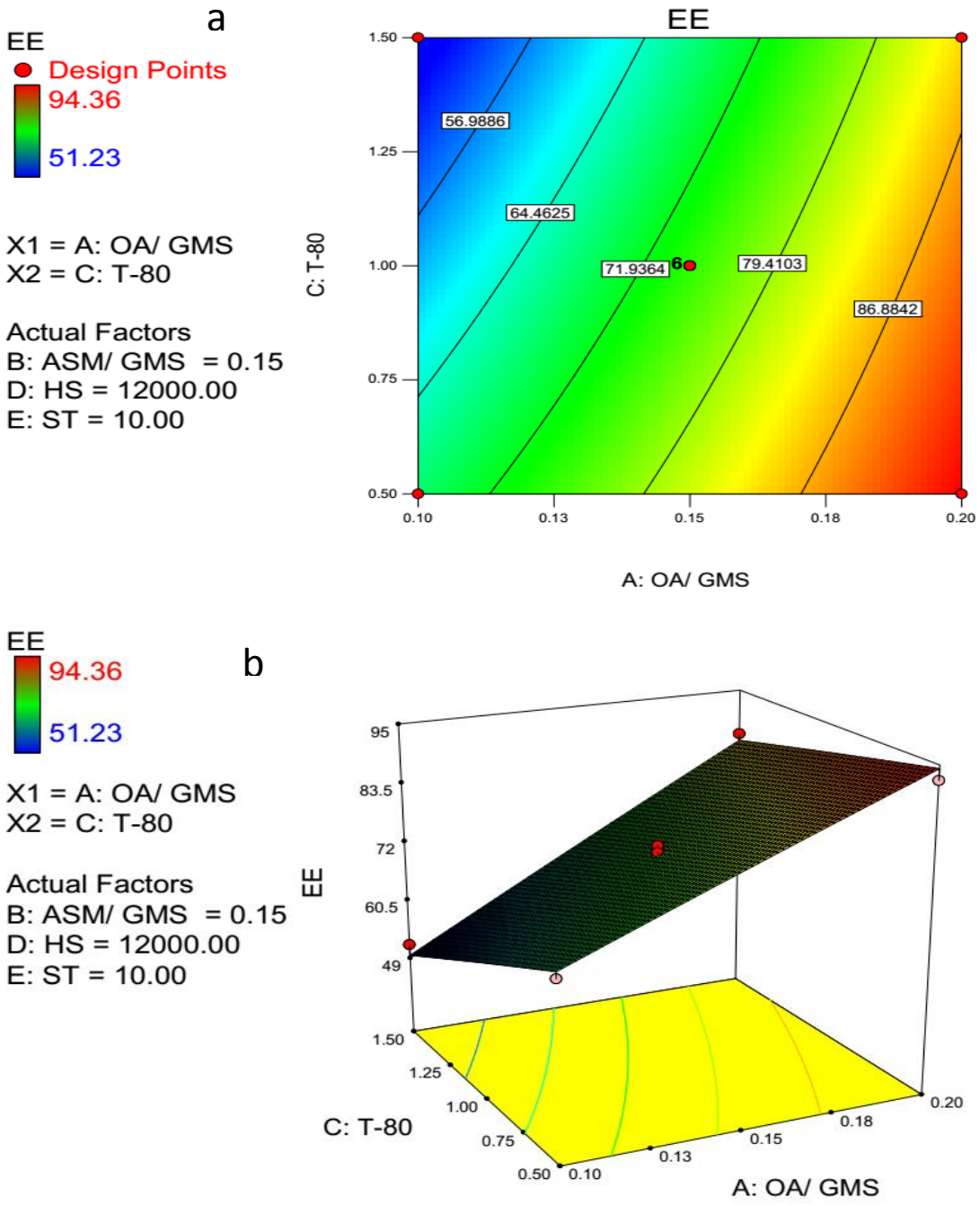

Figure 5.4: 2D (a) and 3D (b) graphical illustrations representing the interaction effect of liquid/solid lipid ratio to surfactant on entrapment efficiency (EE)

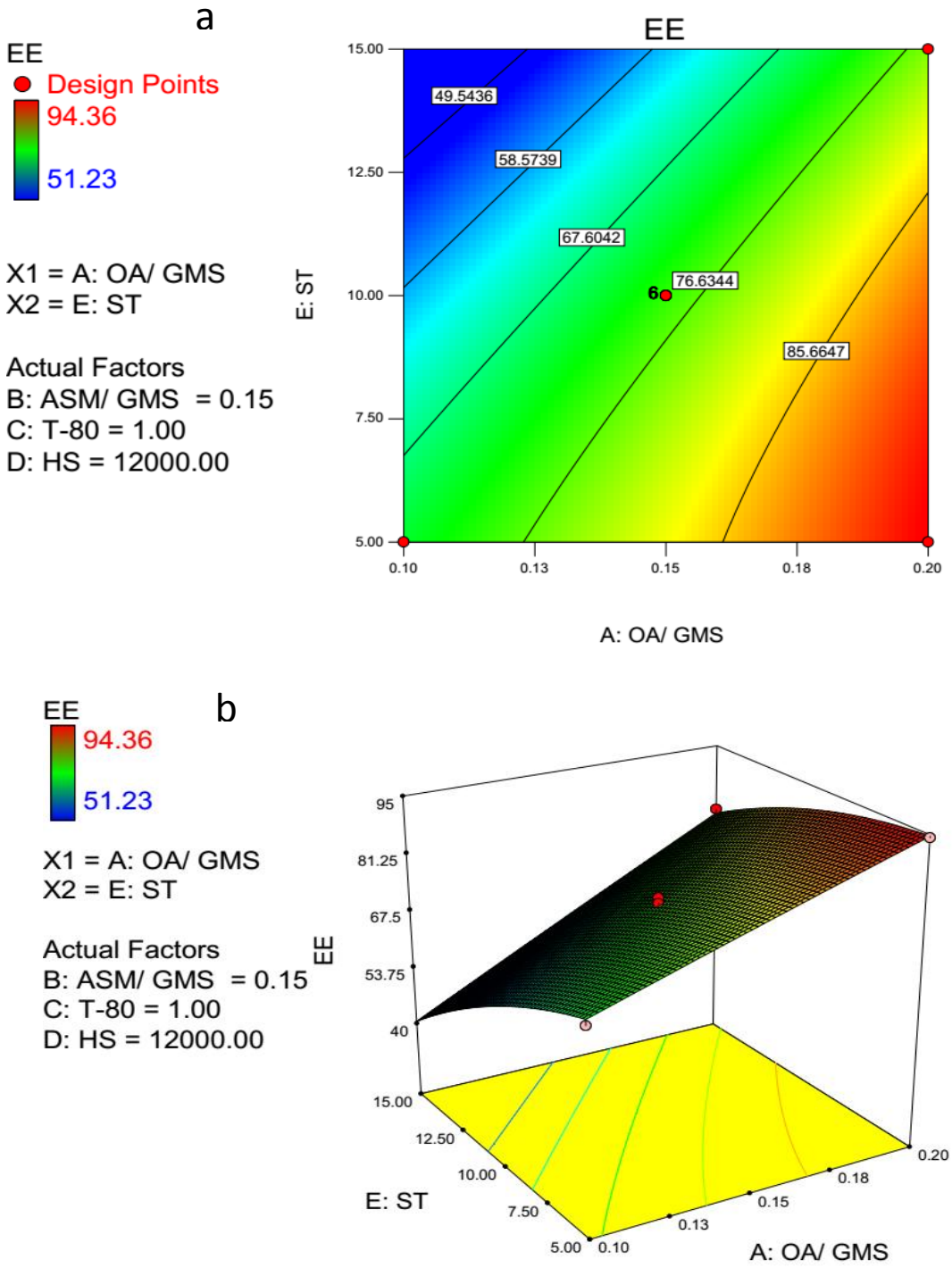

Figure 5.5: 2D (a) and 3D (b) graphical illustrations representing the interaction effect of liquid/solid lipid ratio to sonication time on entrapment efficiency

5.2.3. Risk assessment

Risk assessment is a valuable science-based process used in quality risk management that can aid in identifying which material attributes and process parameters potentially have an effect on product CQAs. For preparation of NLC and their set CQPP, particle size and entrapment efficiency were significantly controlled by selected composition and process variables in defined design space. Moreover, optimum value of PDI could be selected from different solutions appeared in numerical optimization. Linearity in predicted *vs* actual response and symmetrical distribution pattern in residual *vs* predicted, residual *vs* run graph for both particle size, entrapment efficiency suggested that model is fit and the possibility of other missing variables which may be determinant of NLC-CQPP are low (Figure 5.6).

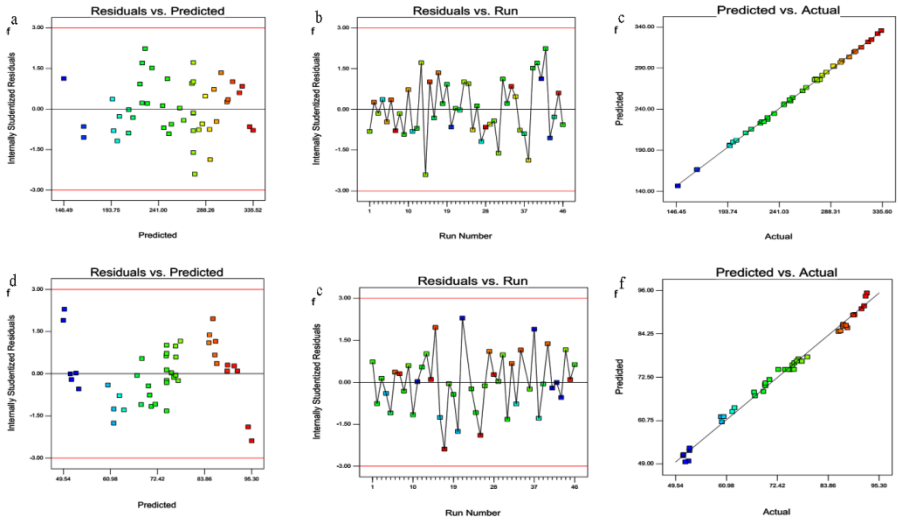

Figure 5.6: Diagnostic illustration graph between predicted vs actual, residual vs predicted and residual vs run for particle size (a-c) and entrapment efficiency (d-e), respectively

5.2.4. Optimization and validation

The optimization of batch was performed by numerical method with maximum desirability factor. The predicted value of PS and EE were found to be 167.54 nm, 83.96%, respectively at A (0.20 w/w), B (0.12 w/w), C (1.50 %w/v), D (15948.27 rpm) and E (5.0 min) as depicted in Figure 5.7. Therefore, a new batch of NLC with the predicted level of independent variables was prepared to confirm the validity of optimization. The observed response of PS and EE were 167.30 ± 7.52 nm and 83.50 ± 2.48%, respectively at set experimental run condition, A = 0.2 w/w, B = 0.10 w/w, C = 1.5 %w/v, D = 16000 rpm and E = 5 min (Table 5.8). The predicted values are in good agreement with observed values demonstrating the reliability of this model in predicting a desirable NLC system for asenapine. The nanoparticles of this size range have been found to be suitable for brain targeting as they preferentially accumulate in brain and demonstrate superior clinical efficacy (Md S *et al.*, 2013; Yang SC *et al.*, 1999). These nanoparticles are transported through blood brain barriers by utilizing different mechanism such as adsorptive transcytosis, inhibition of efflux pumps (p-glycoprotein) and passive diffusion from endothelial cells to the brain cell (Wohlfart S *et al.*, 2012; Wong HL *et al.*, 2012). So, this optimized asenapine loaded nanostructured lipid carriers batch (ANLC) was selected for in-vitro characterization, pharmacokinetic and pharmacological evaluation.

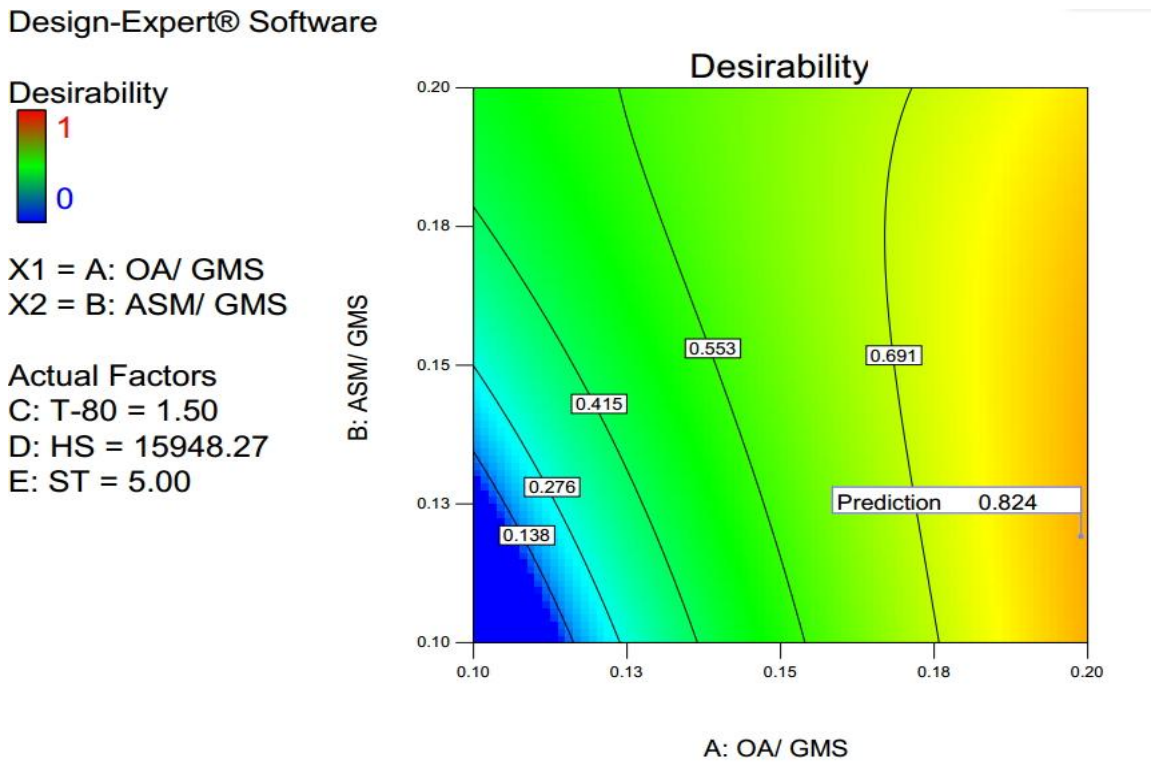

Figure 5.7: Desirability graph for predicted optimized batch

Table 5.8: Optimal predicted and experimental batch with composition and process variables with responses

	Composition and process variables					Response			
Batch	**OA/ GMS (w/w)**	**ASM/ GMS (w/w)**	**Tween-80 (%w/v)**	**HS (rpm)**	**ST (min)**	**PS (nm)**	**EE (%)**	**PDI**	**ZP (mV)**
Predicted	0.20	0.12	1.50	15948	5.00	167.54	83.96	-	-
Experimental (ANLC)	0.20	0.10	1.50	16000	5.00	167.30 ±7.52	83.50 ±2.48	0.261 ±0.024	-4.33 ±1.27

5.3. Characterization of ANLC and GC-ANLC

5.3.1. Particle size, polydispersity index, zeta potential and entrapment efficiency

The particle size, polydispersity index, zeta potential and entrapment efficiency of ANLC are shown in Table 5.8, whereas all these parameters for coated ANLC with different concentration of glycol chitosan are represented in Figure 5.8. As presented in Table 5.8, particle size, zeta potential and entrapment efficiency of ANLC was found to be 167.30 ± 7.52 nm, -4.34 ± 1.27 mV and 83.50 ± 3.48%, respectively. Further, this ANLC was incubated with different concentration of glycol chitosan (0.01, 0.05, 0.1, 0.2 and 0.4 %w/v) to provide optimum coating. Total five different glycol chitosan coated batches (GC 0.01, GC 0.05, GC 0.1, GC 0.2, GC 0.4) were prepared and demonstrated the particle size, zeta potential and entrapment efficiency in the range of 181.58 to 186.97 nm, 5.51 to 18.88 mV and 82.46 to 84.24%, respectively. As specified from the result, a significant increase in the particle size and zeta potential were observed in coated ANLC, where as entrapment efficiency was mostly unaffected. The marginal increase in particle size of coated ANLC may be contributed by polymer coating due to ionic interaction between anionic surface of ANLC and cationic glycol chitosan. The zeta potential is one of the fundamental parameter to evaluate stability of colloidal system. However, it foremost depends on the chemical nature and interaction between lipid, surfactant and drug. The negative potential and low value of zeta potential justifies acidic nature of lipid matrix and nonionic nature of surfactant, respectively. Normally,

colloidal dispersion with zeta potential above the range of -30 to +30 mV is considered as stable. But, this empirical rule does not apply to steric stabilization provided by Tween-80, which continues to stabilize the particles even under low values of zeta potential due to shift in shear plane of particles (Redhead HM *et al.*, 2001). The positive value of surface charge (+5.51 to +18.88) due to cationic charge of glycol chitosan polymers over ANLC showed concentration dependent increase in zeta potential upto 0.2% w/v. These results indicated that glycol chitosan was reached to saturated level at 0.2% w/v and further excess amount of glycol chitosan could not change the coating strength as well as zeta potential of coated ANLC. These higher zeta potential gave additive effect on the stability of GC-ANLC apart from steric/surface stabilization provided by Tween-80. Meanwhile, entrapment efficiency was not significantly altered among uncoated and coated ANLC. This insignificant difference in entrapment efficiency suggested that glycol chitosan coating do not alter the drug solubility, miscibility, physical and chemical structure of lipid matrix as well as it indicated the high compatibility of asenapine with glyceryl monostearate and oleic acid to accommodate large amount of drug without any interference from surface modification. Indeed, ANLC coated with 0.2 %w/v glycol chitosan was selected as best batch (particles size (184.20 ± 5.59 nm), zeta potential (18.82 ± 1.18 mV), polydispersity index (0.293 ± 0.034) and entrapment efficiency (83.52 ± 2.59%)) for the next study considering and was further denoted as GC-ANLC.

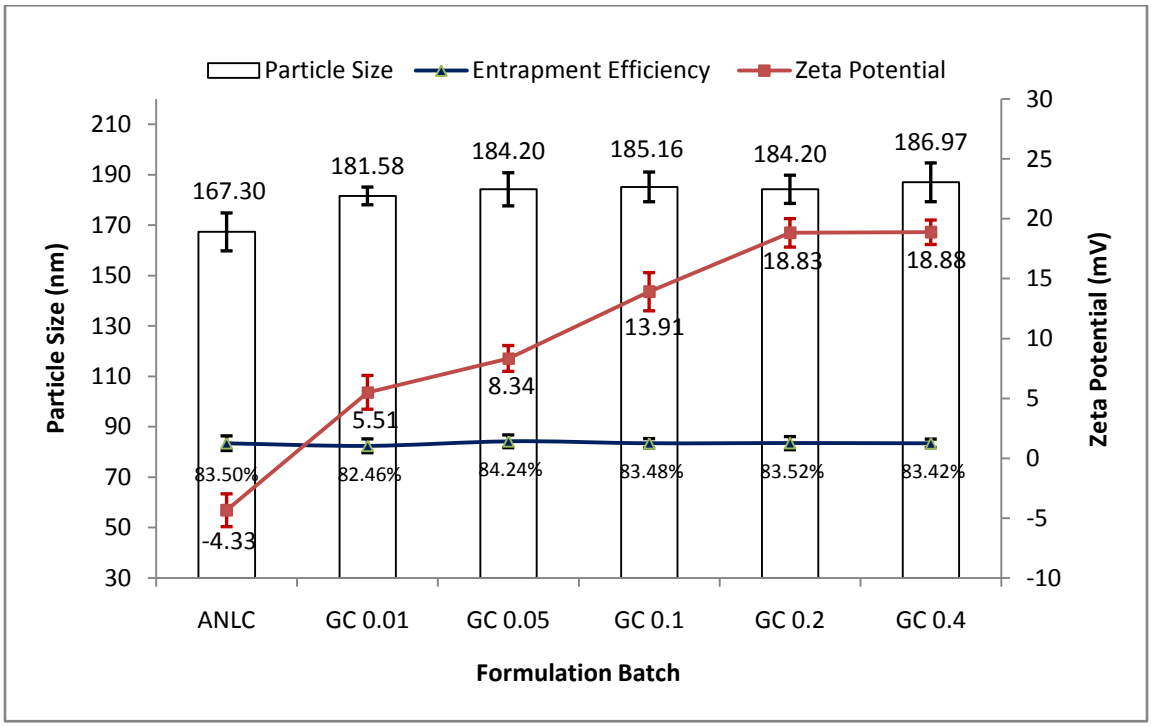

Figure 5.8: Graphic illustrating particle size, zeta potential and entrapment efficiency of ANLC and coated ANLC with different concentration of glycol chitosan (0.01, 0.05, 0.1, 0.2 and 0.4 w/v), mean±SD, n= 3

5.4. *In-vitro* drug release study

The *in-vitro* drug release of ASM and ANLC are depicted in Figure 5.9. The ASM produced more than 50% drug release in 3 h and approximate 90% in 12 h. The release study of ANLC demonstrated the biphasic release pattern, burst release followed by sustained release of drug upto 24 h study. Initial burst release may be attributed to presence of adsorbed free drug or liquid lipid soluble drug on outer surface, which accounts for quick release into the surrounding media. Further, sustained release pattern was contributed by the entrapped drug inside lipid matrix. The release profile of the asenapine from ANLC was fitted into the Zero order (r^2 = 0.7962, AIC= 80.89), First order (r^2 = 0.9328, AIC= 68.69), Higuchi (r^2 = 0.9895, AIC= 49.32), Korsmeyer-Peppas (r^2 = 0.9911, n = 0.53, AIC= 48.48) and Hixson-Crowell (r^2 = 0.9896, AIC= 72.36) release kinetics model. Based on high coefficient of correlation and low AIC (Akaike information criterion) value, the Korsmeyer-Peppas model was found to be best fit model. It indicates that the drug release follows the anomalous transport (n value between 0.5-1.0) of drug i.e. release mechanism is not well known or more than one type of release phenomena could be involved (Costa P and Sousa Lobo JM, 2001).

Similarly, as shown in Figure 5.10, GC-ANLC demonstrated around 50%, 90% drug release in 12 h and 24 h, respectively. The cumulative percent release of asenapine from GC-ANLC was calculated at each time point and it was fitted into the Zero order (r^2= 0.9734, AIC= 82.96), First order (r^2= 0.9847, AIC= 69.86), Higuchi (r^2= 0.9938, AIC= 52.94), Korsmeyer-Peppas (r^2= 0.9937, n=0.528, AIC= 53.84) and Hixson-

Crowell (r^2= 0.9844, AIC= 73.67) release kinetics model. Based on the high r^2 (regression coefficient) and low AIC value, Higuchi model was found to be best fit drug release kinetic model for describing the release of asenapine form lipid matrix of GC-ANLC. However, ANLC demonstrated Korsmeyer-Peppas release model. These differences in release kinetics between ANLC and GC-ANLC revealed that glycol chitosan act as a diffusion layer for the release of asenapine from GC-ANLC matrix. From Korsmeyer-Peppas equation of GC-ANLC, n value indicated that drug release follows the anomalous transport (n value between 0.5 and 1.0) of drug.

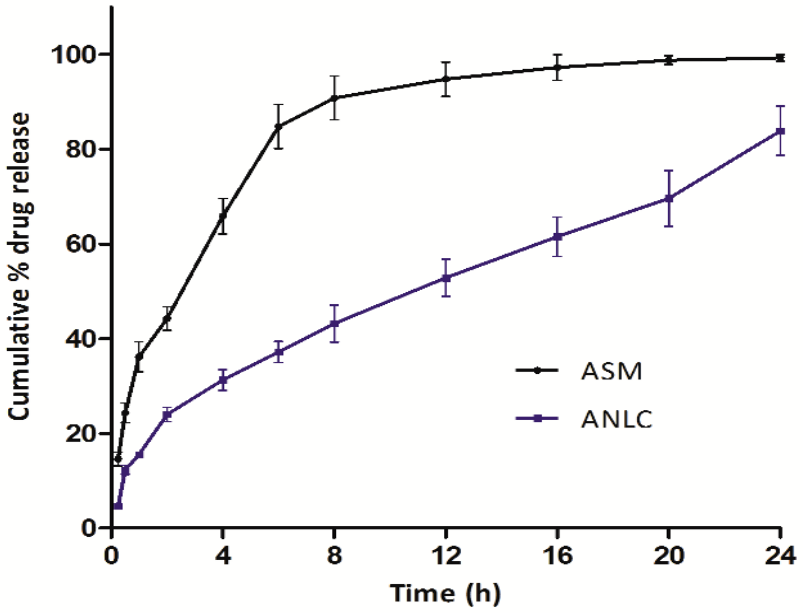

Figure 5.9: *In-vitro* drug release profile of ASM and ANLC in phosphate buffer pH 7.4. (mean ± SD, n=3)

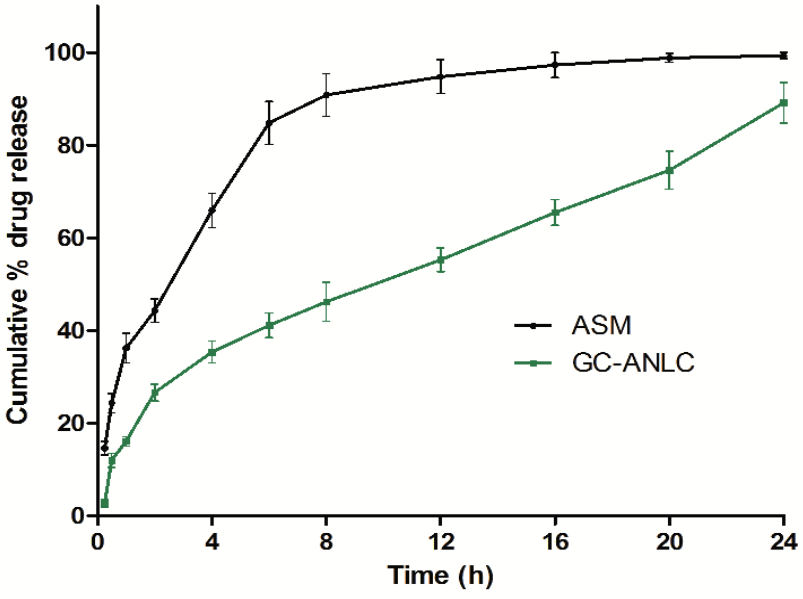

Figure 5.10: *In-vitro* drug release profile of ASM and GC-ANLC in phosphate buffer pH 7.4. (mean ± SD, n=3)

5.5. Solid state characterization

5.5.1. Fourier transform infrared spectroscopy

The overlay spectrum of ASM, GMS and ANLC are shown in Figure 5.11 whereas the IR spectra of ASM, GMS, GC and GC-ANLC are presented in Figure 5.12. The IR spectrum of asenapine maleate revealed the characteristics absorption bands at 653.89 cm^{-1} (C-Cl), 1192.67 cm^{-1} (C-O-C), 1251.84 cm^{-1} (-N<, 3°amine), 1573.97 cm^{-1} (C-C, aromatic ring), 1705.13 cm^{-1} (-C=O), 3037.99 cm^{-1} (-O-H). However, all the characteristic peaks of ASM could not be included for interaction study in ANLC GC-ANLC owing to similarity in some of functional groups common to GMS, Oleic acid and Tween 80. The characteristic peak at 666.39 cm^{-1}, 1249.91 cm^{-1} and 1579.75 cm^{-1} for ANLC and 658.39 cm^{-1}, 1253.23 cm^{-1}, and 1572.61 cm^{-1} for GC-ANLC corresponding to ASM characteristic peak at 653.89 cm^{-1}, 1251.84 cm^{-1} and 1573.97 cm^{-1} confirms the presence of asenapine maleate in nanostructure lipid carriers. It indicated that no chemical or ionic interaction between the drug and lipid matrix of ANLC and GC-ANLC. The slight shifting of absorption bands of ASM in nanostructured lipid carriers can be attributed to change in molecular environment and intermolecular interactions associated with dispersed drug molecule in lipid excipients.

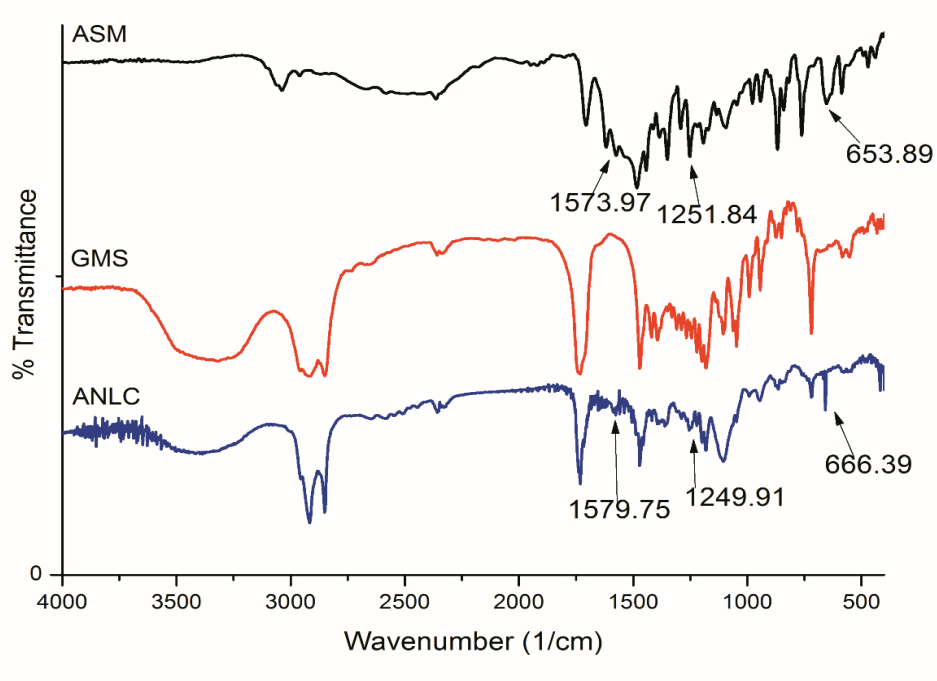

Figure 5.11: FTIR spectra of ASM, GMS and ANCL

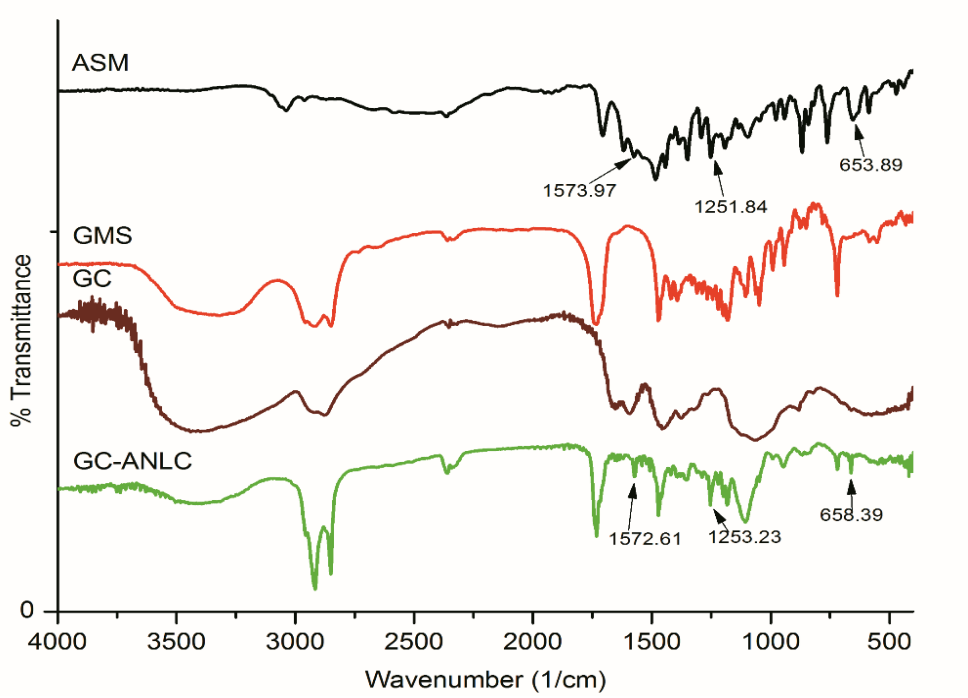

Figure 5.12: FTIR spectra of ASM, GMS, GC and GC-ANCL

5.5.2. Differential scanning calorimetry

DSC thermogram of ASM, GMS with ANLC and GC-ANLC are shown in Figure 5.13 and 5.14, respectively. A sharp endothermic peak in ASM (T_{onset} = 138.71 °C, ΔH = 72.71 J/g) and GMS (T_{onset} = 46.93 °C, ΔH = 172.9 J/g), corresponding to its melting point demonstrated crystalline nature of these substances. However, GC did not show any distinct endothermic peak over the entire range of the tested temperatures (5–167°C), confirming amorphous nature of this polymer (Figure 5.14). A broad asymmetric melting peak was observed in the thermogram of ANLC (T_{onset} = 36.01 °C, ΔH = 86.23 J/g) and GC-ANLC (T_{onset} = 34.52 °C, ΔH= 87.21 J/g). The lack of ASM melting peak in ANLC and GC-ANLC may be attributed to molecularly dispersed state of asenapine maleate in lipid matrix. The presence of broader endothermic peak below the melting point of GMS correlated with possible effects of liquid lipid and surfactant on crystal lattice of GMS (Das S *et al.*, 2012). Further, particle size also has pronounced effect on the melting endotherm of lipid in nanosize range. (Bunjes H and Unruh T, 2007). The different lipid nanoparticles melt at different temperatures which results in peak broadening and shift in melting transition at lower temperature as compared to bulk lipid.

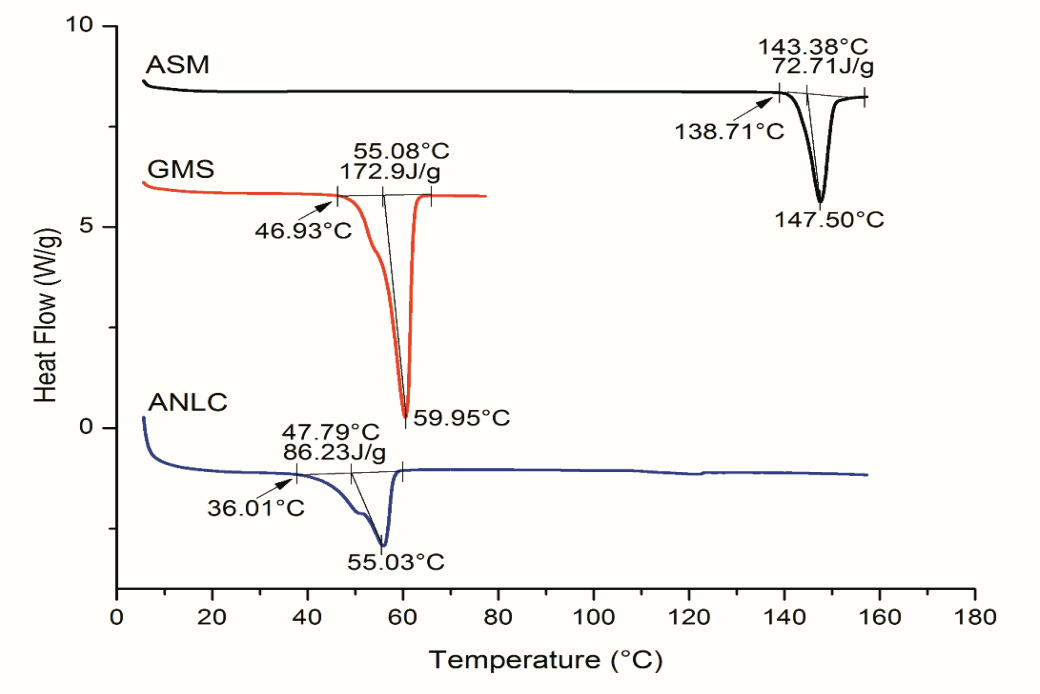

Figure 5.13: DSC spectra of ASM, GMS and ANCL

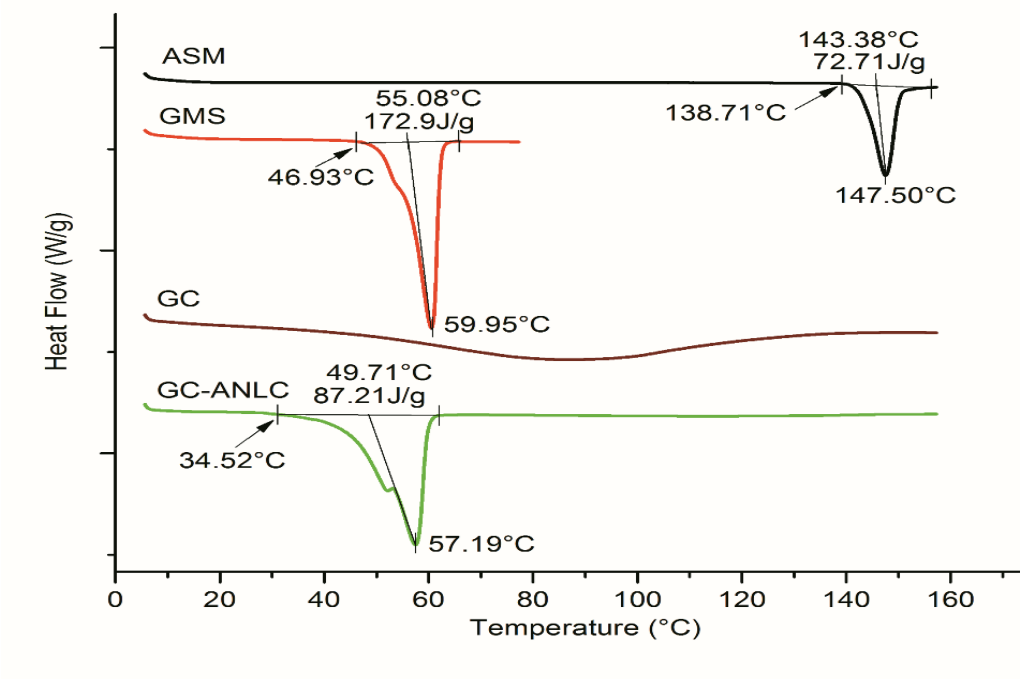

Figure 5.14: DSC spectra of ASM, GMS, GC and GC-ANCL

5.5.3. X-Ray diffraction

XRD is a non destructive analytical technique with broad range of application. This technique is based on Bragg's Law, observing the scattered intensity of an X-ray beam hitting a sample as a function of incident and scattered angle, polarization and wavelength or energy. The positions and the intensities of the peaks are used for identifying the structure of the material. XRD overlay spectra of ASM, GMS and ANLC are shown in Figure 5.15. Similarly, overlay spectra of ASM, GMS, GC and GC-ANLC are depicted in Figure 5.16. The XRD diffraction pattern of ASM exhibit sharp peaks at 2θ angle 14.4, 16.0, 16.6, 18.3, 19.4, 20.2, 21.8, 23.2, 23.8, 25.0, 26.0 and 26.6 degree which demonstrates crystalline nature of drug. Further, bulk GMS in crystalline form exhibited 2θ angle characteristic peaks at 19.3, 22.7 and 23.3 degree. The diffraction pattern of ANLC and GC-ANLC resembles to GMS with total absence of 2θ characteristic peak of asenapine. The changes in the position of peaks were also depending on factors such as particle size, quantity of sample and formulation additives (Ramalingam P and Ko YT, 2015). These patterns suggested amorphous nature of asenapine in lipid matrix with significant distortion in crystal lattice of GMS. The amorphous asenapine in ANLC and GC-ANLC was good for stability due to less expulsion of the encapsulated drug during storage (Rahman HS *et al.*, 2013). The XRD data for ASM, GMS, ANLC and GC-ANLC were good agreement with DSC results.

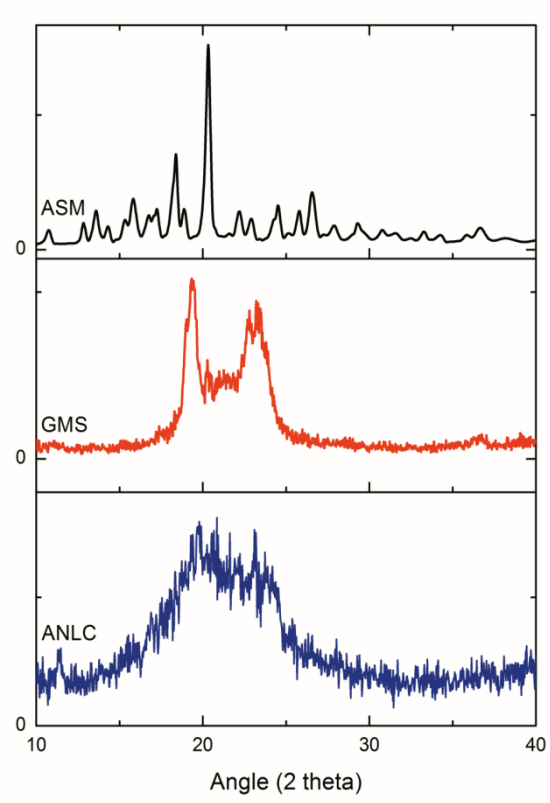

Figure 5.15: XRD spectra of ASM, GMS and ANCL

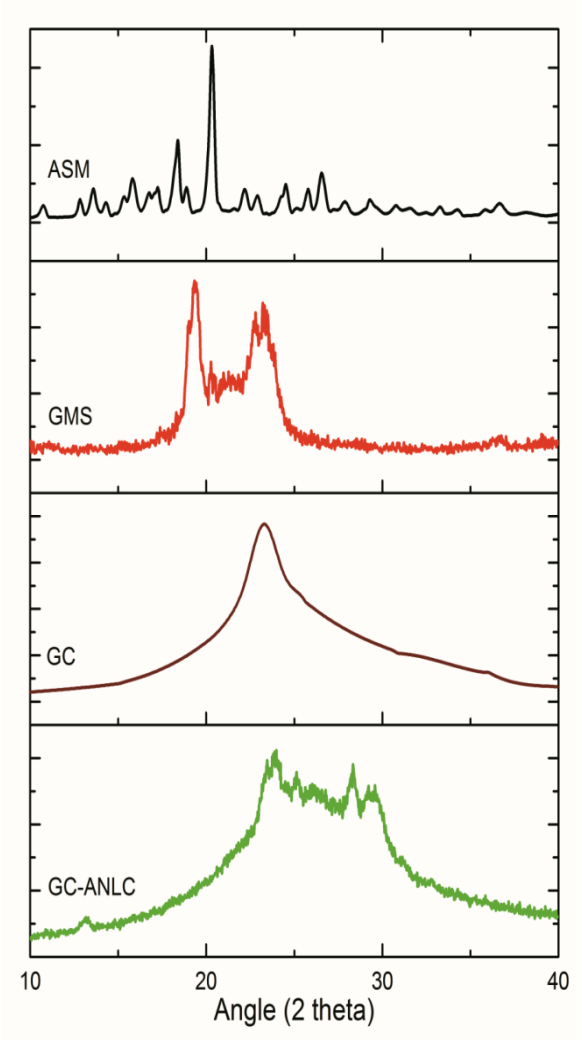

Figure 5.16: XRD spectra of ASM, GMS, GC and GC-ANCL

5.6. Surface characterization

5.6.1. Transmission electron microscopy

Transmission electron microscopy (TEM) of ANLC (Figure 5.17) indicated distinct clear spherical particles size, which was close to the results obtained by dynamic light scattering (DLS) method. Moreover, the actual particle size reported by TEM was found to be less than dynamic light scattering results. It is postulated that these differences were shown by difference in size measurement methodology. The solvent layer attached to particle; called hydrodynamic size is measured in DLS, which is always greater than actual particle size measured by TEM. The electron diffraction ring pattern of ANLC as indicated in Figure 5.18 confirmed the amorphous nature which was in consistent with those obtained from the DSC and XRD results. The surface morphological study by TEM of GC-ANLC (Figure 5.19) indicates that spherical and uniform shape with non agglomerated particles. The particle size of GC-ANLC was found to in the range of 150-200 nm. Further, presence of glycol chitosan coating surrounding the lipid matrix was well visualized on the surface of GC-ANLC in the form of diffuse peripheral structure where as ANCL indicated solid matrix. Similar to ANLC, electron diffraction ring pattern of GC-ANLC (Figure 5.20) also confirmed the amorphous nature of lipid matrix supported by diffuse ring structure.

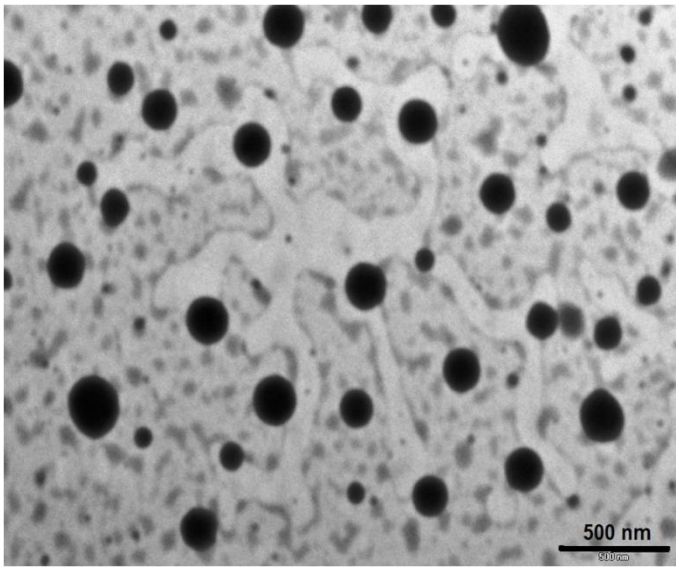

Figure 5.17: Transmission electron micrograph of ANLC

(Scale bar represents 500 nm)

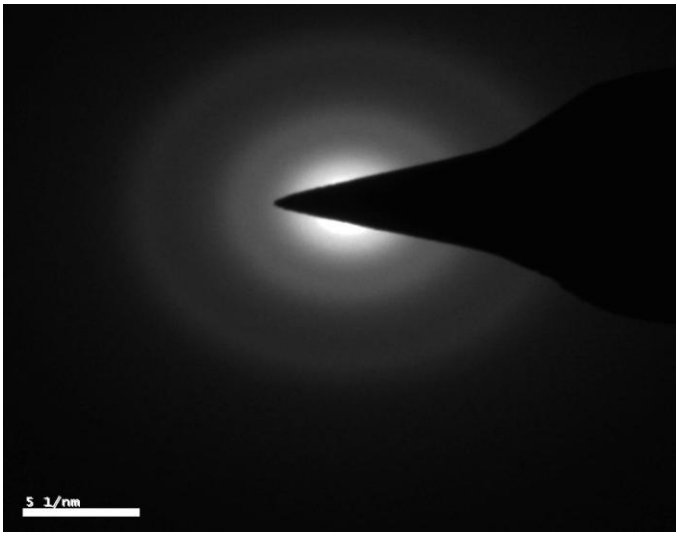

Figure 5.18: Electron diffraction ring pattern of ANCL

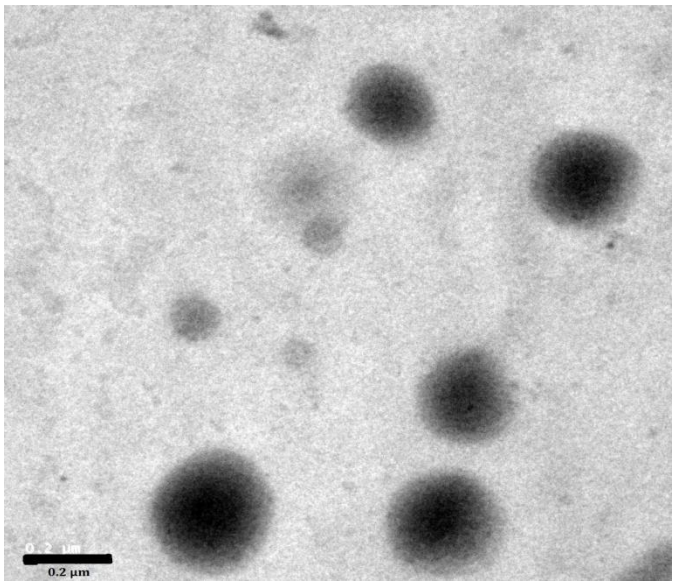

Figure 5.19: Transmission electron micrograph of GC-ANLC

(Scale bar represents 200 nm)

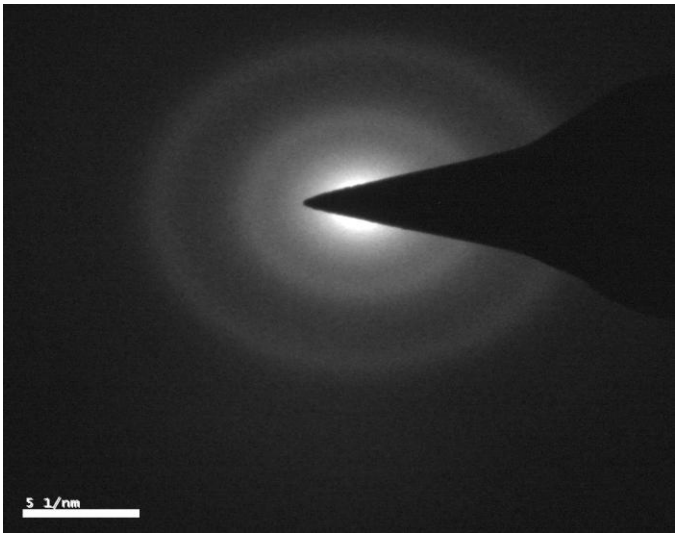

Figure 5.20: Electron diffraction ring pattern of GC-ANCL

5.6.2. Atomic force microscopy

Atomic force microscopy was carried out to characterize the surface morphology of ANLC and GC-ANL. As indicated in Figure 5.21 and Figure 5.22, most of the particles were spherical with a smooth surface. AFM image of both ANLC and GC-ANLC were in good agreement with size determined by dynamic light scattering and transmission electron microscopy methods. Shape parameters were compared by determining average roughness, kurtosis and skewness of batches. Kurtosis indicated whether the data are heavy-tailed or light-tailed relative to a normal distribution. That is, data sets with high kurtosis tend to have heavy tails, or outliers. Data sets with low kurtosis tend to have light tails, or lack of outliers. Skewness is a measure of symmetry, or more precisely, the lack of symmetry. If skewness is positive, the data are positively skewed or skewed right, meaning that the right tail of the distribution is longer than the left. If skewness is negative, the data are negatively skewed or skewed left, meaning that the left tail is longer. Zero value of skewness indicates perfectly symmetrical data (Hembree B, 2013). Shape parameters of ANLC exhibited 2.896 nm, 4.60 and 0. 211 value as average roughness, kurtosis and skewness, respectively. Moreover, GC-ANLC showed average roughness, kurtosis and skewness value as 9.994 nm, 5.052 and 0.581, respectively. Overall these values indicated particles are smooth with almost symmetrical distribution. When comparing both ANLC and GC-ANLC, surface coating with glycol chitosan provided a rougher surface with higher and sharper central peak, and longer and fatter tails compared to uncoated nanoparticles.

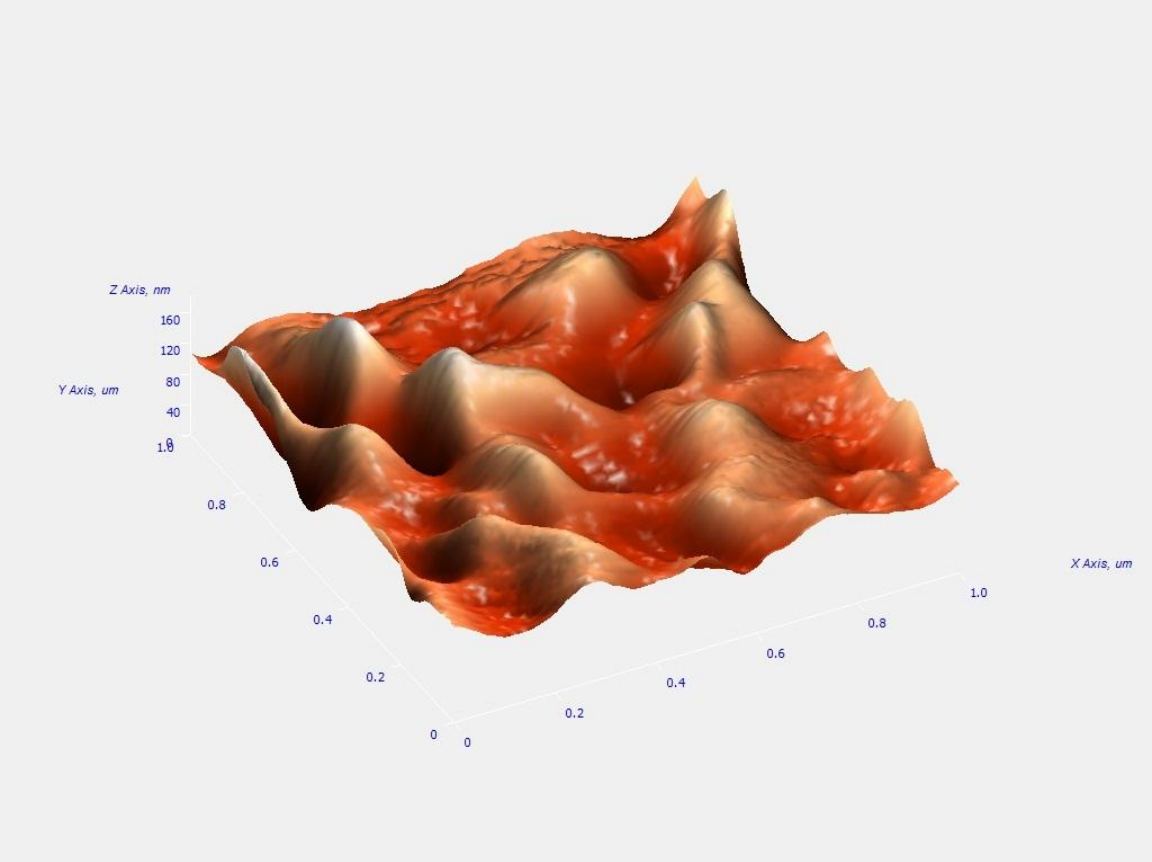

Figure 5.21: Atomic force micrograph of ANLC

(Measurement scale: 1 µm X 1 µm X 160 nm)

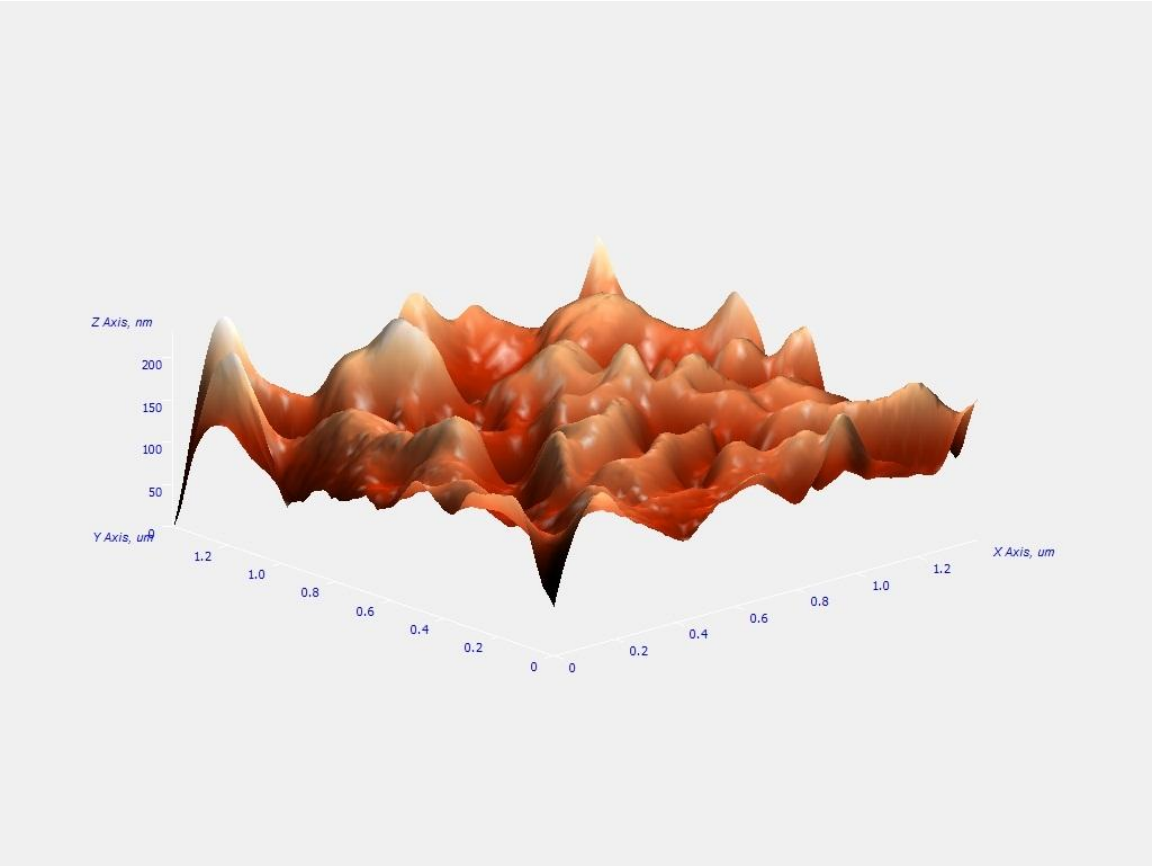

Figure 5.22: Atomic force micrograph of GC-ANLC

(Measurement scale: 1.2 µm X 1.2 µm X 200 nm)

5.7. Stability study

The results of the stability study of ANLC are presented in Table 5.9. As shown in table, particle size increases while zeta potential and entrapment efficiency decreases with time. However, the statistical analysis indicated that these changes were not significant (p>0.05). In the same way, also the particle size, zeta potential and entrapment efficiency of GC-ANLC (Table 5.10) did not changed significantly (p>0.05) with time during stability testing period. The release profile of ANLC (Figure 5.23) and GC-ANLC (Figure 5.24) on day 0, 30, 60 and 90 were compared by difference factor (f_1) and similarity factor (f_2) considering 0 day releases as reference. Generally, f_1 values lower than 15 (0-15) and f_2 values higher than 50 (50-100) demonstrated similarity of dissolution profile. The observed f_1 values (ANCL: 3.48-6.77, GC-ANLC: 4.82-9.38) and f_2 values (ANLC: 75.31-85.95, GC-ANLC: 71.58-80.14) justified the similarity of release profile of ANLC and GC-ANLC during storage period. These finding indicates that the optimized ANLC and GC-ANLC were physically stable with no aggregation and similarity in drug release pattern during 90 days of stability period.

Table 5.9: Stability studies of ANLC

Day	Particle Size (nm)	Zeta Potential (mV)	Entrapment Efficiency (%)	*In-vitro* release profile comparison	
				f_1	f_2
0	167.30 ± 7.52	-4.33 ± 1.27	83.50 ± 2.48	Reference	Reference
30	168.26 ± 7.33	-4.51 ± 0.36	83.36 ± 3.22	3.48	85.95
60	172.91 ± 5.21	-3.96 ± 1.70	82.37 ± 2.81	5.72	78.34
90	175.21 ± 3.88	-3.69 ± 1.19	82.04 ± 2.06	6.77	75.31

f1: difference factor; f2: similarity factor, mean±SD, n=3.

Table 5.10: Stability studies of GC-ANLC

Day	Particle Size (nm)	Zeta Potential (mV)	Entrapment Efficiency (%)	*In-vitro* release profile comparison	
				f_1	f_2
0	184.29 ± 5.59	18.82 ± 1.18	83.50 ± 2.59	Reference	Reference
30	185.28 ± 5.73	18.75 ± 0.96	82.78± 2.26	4.82	80.14
60	186.64 ± 9.30	18.69 ± 1.82	82.02 ± 2.92	6.67	72.47
90	187.49 ± 12.0	18.26 ± 1.36	81.99 ± 2.60	9.38	71.58

f1: difference factor; f2: similarity factor, mean±SD, n=3.

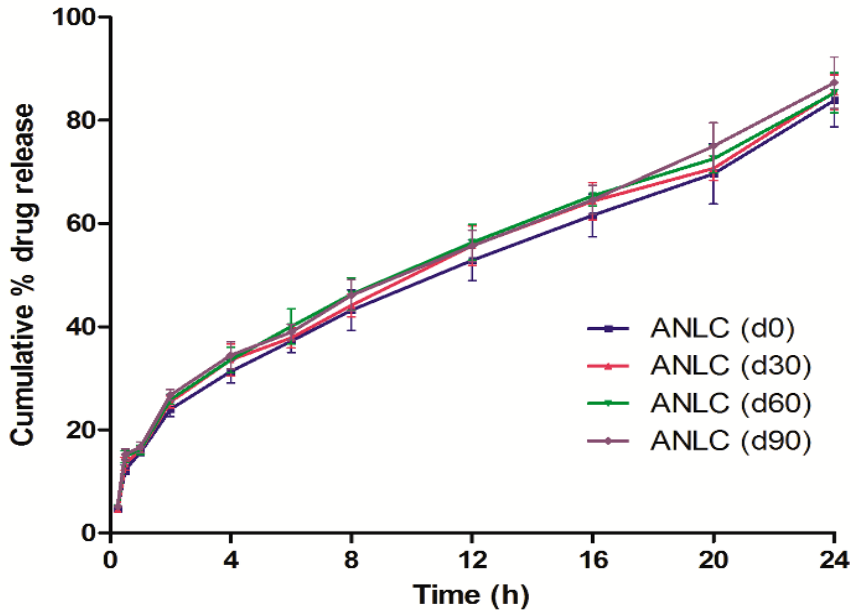

Figure 5.23: In-vitro release of drug from ANLC at 0 day (d0), 30 days (d30), 60 days (d60) and 90 days (d90)

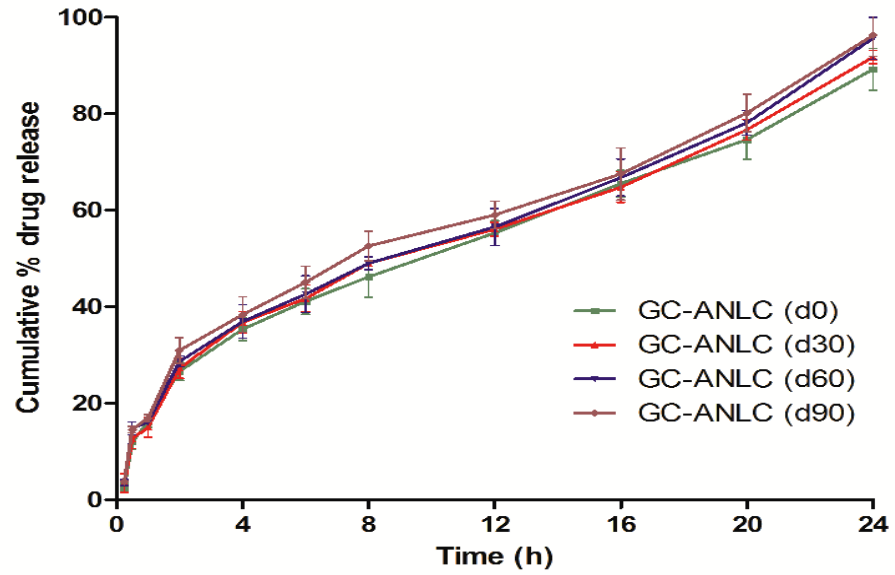

Figure 5.24: In-vitro release of drug from GC-ANLC at 0 day (d0), 30 days (d30), 60 days (d60) and 90 days (d90)

5.8. *In-vitro* cell viability study

As shown in Figure 5.25, more than 95% cell viability was found at tested concentration (0.001-10 µM asenapine) of ASM, ANLC and GC-ANLC. The results of cell viability in MTT assay demonstrated no significant difference in % viability in group treated with ASM, ANLC and GC-ANLC ($p>0.05$) compared to control.

It is clear from the cell compatibility study that both ASM and GC-ANLC did not significantly affect the cells viability. This study indicates that chemical composition of ANLC and GC-ANLC were well tolerated and do not form any toxic product.

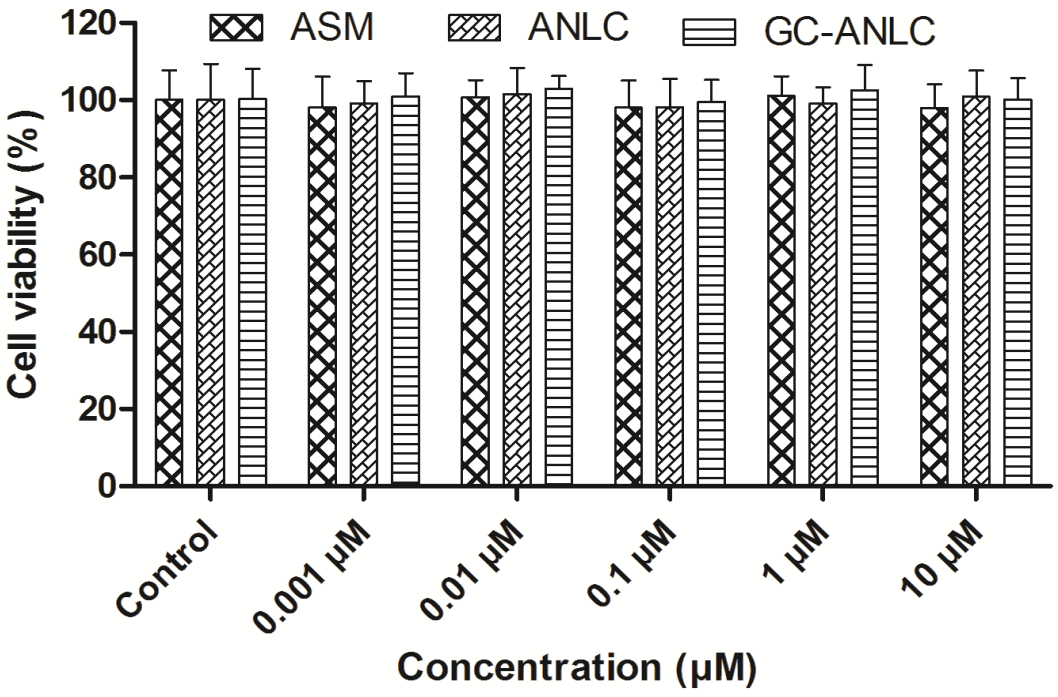

Figure 5.25: Cell viability results of ASM, ANLC and GC-ANLC

5.9. *In-vivo* pharmacokinetic study

Different pharmacokinetic parameters of ANLC and GC-ANLC were evaluated to observe the absorption and disposition of asenapine through nasal route. Drug concentration-time profiles of ANLC compared to ASM in brain and plasma are shown in Figure 5.26. The pharmacokinetic parameters obtained from these profiles are presented in Table 5.11. ANLC showed significantly higher ($p<0.05$) C_{max} (74.13 ± 6.73 ng/ml), $AUC_{0\text{-}24h}$ (560.93 ± 27.85 h.ng/ml) and MRT (7.1 ± 0.13 h) in brain compared to pure drug (ASM) when both were administered by i.n. route. All these contributed to 1.34 and 2.68 times higher bioavailability of drug by ANLC in plasma and brain, respectively after i.n. administration. This can be attributed to the nanosize of the carriers as well as presence of oleic acid (liquid lipid) and Tween 80 (surfactant) which causes to enhancement of permeation of ANLC across the respiratory epithelium and vessels fenestrating the brain. These finding is in conformation with earlier reports for brain targeting potential of nanoparticles by Tween 80 (Kreuter J, 2001; Wilson B *et al.*, 2008). After i.n. administration, delivery of the drug to brain has pronged approach, one through olfactory and trigeminal neural pathways and another after permeation from respiratory epithelium to blood and then to brain (Haque S *et al.*, 2012; Thorne RG *et al.*, 2004). This could be further related with the higher drug targeting efficiency (2.07) of ANLC to brain via i.n. route. In contrast, ASM through i.v. route elicited significantly higher C_{max} (82.76 ± 14.78 ng/ml) in plasma compared to ANLC and ASM via i.n. route owing to instantaneous availability of all free drugs in systemic circulation. Higher $AUC_{0\text{-}24h}$

and MRT of ANLC indicates that drug remains in the brain and blood for longer period of time due to sustained release of drug from lipid matrix. The results obtained from above study suggested about the potential of ANLC for brain targeting.

Table 5.11: Pharmacokinetic parameters data of ASM (i.v., i.n.), ANLC (i.n.) and GC-ANLC in CF rats.

PK parameters	Organ	ASM (i.v.)	ASM (i.n.)	ANLC (i.n.)	GC-ANLC (i.n.)
C_{max} (ng/ml)	Plasma	82.76 ± 14.78	33.65 ± 15.52[a]	41.76 ± 3.47[a]	44.12 ± 2.92[a]
	Brain	41.46 ± 7.57	53.34 ± 9.76	74.13 ± 6.73[a,b]	94.93 ± 11.73[a,b,c]
T_{max} (h)	Plasma	0.17 ± 0	0.5 ± 0[a]	0.5 ± 0[a]	0.5 ± 0[a]
	Brain	2.0 ± 0	2.0 ± 0	1.0 ± 0[a,b]	1.0 ± 0[a,b]
$AUC_{0\text{-}24h}$ (h.ng/ml)	Plasma	115.63 ± 25.53	68.25 ± 21.34[a]	154.46 ± 10.61[a,b]	163.62±10.79[a,b]
	Brain	202.70 ± 35.65	209.42 ± 42.48	560.93 ± 27.85[a,b]	826.81±78.29[a,b,c]
MRT (h)	Plasma	2.1 ± 0.28	2.0 ± 0.23	5.3 ± 0.18[a,b]	5.84 ± 0.21[a,b]
	Brain	3.0 ± 0.21	2.8 ± 0.26	7.1 ± 0.13[a,b]	10.31 ± 0.63[a,b,c]
Absolute bioavailability (%)	Plasma	-	59.02	133.58	141.50
	Brain	-	103.31	276.72	407.89
DTE			1.75	2.07	2.88

The parameters C_{max}, T_{max}, $AUC_{0\text{-}24h}$, and MRT of groups were compared by one way ANOVA followed by Tukey's post-hoc test; a ($p<0.05$) compared to ASM (i.v.); b ($p<0.05$) compared to ASM (i.n.); c ($p<0.05$) compared to ANLC (i.n.); mean±SD, n=5.

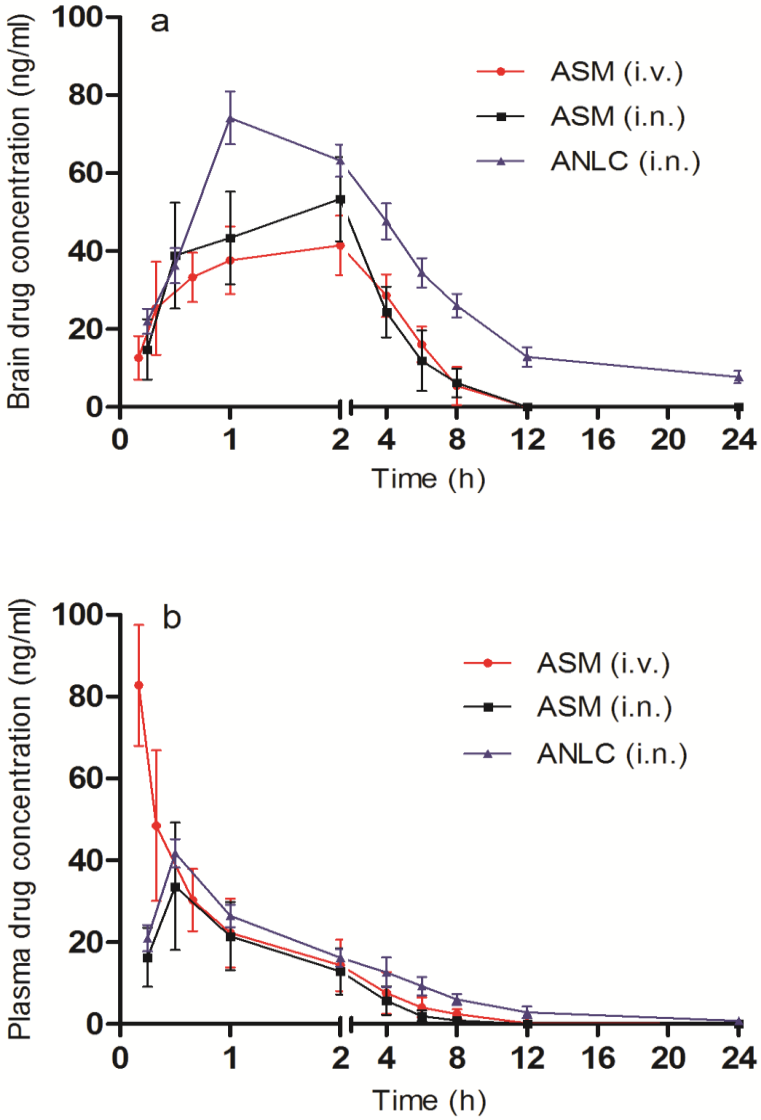

Figure 5.26: *In-vivo* brain uptake and pharmacokinetic study. Brain (a) and plasma (b) drug concentration time profile of ASM (via i.v. and i.n.) and ANLC (via i.n.) route. mean±SD, n=5.

Further, asenapine concentrations in plasma and brain homogenate were measured to determine in-vivo outcome of glycol chitosan coated nanocarriers on pharmacokinetic parameters. Drug concentration-time profiles of GC-ANLC compared to ASM in brain and plasma are shown in Figure 5.27 and their corresponding plasma and brain pharmacokinetic parameters are shown in Table 5.11. The plasma pharmacokinetic results showed that no significant difference ($p>0.05$) were observed among ASM (C_{max}: 33.65 ± 15.52 ng/ml, T_{max}: 0.5 h) and GC-ANLC (C_{max}: 44.12 ± 2.92 ng/ml, T_{max}: 0.5 h) in C_{max} and T_{max} via intranasal route but these groups showed significantly difference ($p<0.05$) with i.v. administered ASM (C_{max}: 82.76 ± 14.78 ng/ml, T_{max}: 0.17 h). As shown in Table 5.11, ASM (i.v.) and GC-ANLC (i.n.) demonstrated higher C_{max} in plasma and brain within 10 min and 1 h, respectively. This higher plasma C_{max} in ASM (i.v.) was contributed by lack of absorption phase as well as instantaneous availability of total drug in systemic circulation. However, higher C_{max} in brain of GC-ANLC group might be contributed by nano size carriers which cross through the olfactory epithelium and reached to CNS via olfactory and trigeminal neural pathway without interference from BBB. In addition to this, the positive charges of glycol chitosan due to its amino groups at surface of the particle interact with oppositely charge mucin at nasal mucosa provides in longer residence time for absorption.

The plasma $AUC_{0\text{-}24h}$ (163.62 ± 10.79 h.ng/ml) of GC-ANLC was significantly higher ($p<0.05$) than those observed in ASM after i.v. and i.n. administration. The absolute

systemic bioavailability of GC-ANLC (141.50%) demonstrated approximately ~2.3 times higher compared to ASM (59.02%) after i.n. delivery.

In order to verify the potential of GC-ANLC after i.n. administration in brain targeting, brain samples were assessed for asenapine concentration at different time points and compared with i.v. and i.n. administered ASM. As shown in Table 5.11, C_{max} and $AUC_{0\text{-}24h}$ of GC-ANLC after i.n. administration was found to be 94.93 ± 11.73 ng/ml and 826.81 ± 78.29 h.ng/ml, respectively, which was significantly higher to ASM via both i.v. and i.n. routes. The greater availability of GC-ANLC in brain may be due to presence of Tween 80 which contributed in crossing BBB by endocytosis mechanism (Kreuter et al., 2003, Wilson et al., 2008).

When comparing the drug concentration - time curve of blood and brain, except first two few time points, no significance differences in asenapine concentration at different time point were observed between ASM (i.v.) and ASM (i.n.) which indicates that elimination process of free drug was not going to change after i.v. and i.n. administration. However, GC-ANLC could protect asenapine from enzymatic degradation as well as prevent its uptake from macrophages due to hydrophilic chain of glycol chitosan and Tween-80 at surface. That results in higher brain accumulation and long systemic circulation which was evident by availability of drug upto 24 h. All these favorable properties of GC-ANLC result in significantly higher ($p<0.05$) $AUC_{0\text{-}24h}$ in blood and brain than those of ASM (i.v.) and ASM (i.n.) and especially in brain, it was approximately 4 times higher. Indeed, higher $AUC_{0\text{-}24h}$ of GC-ANLC in plasma suggests that absorption of GC-ANLC could not only occur

through olfactory epithelium but also from respiratory epithelium which favors the systemic absorption (Haque et al., 2012). Also, it may be postulated that presence of oleic acid in lipid matrix, which is reported as penetration enhancer contributed in higher availability of asenapine in GC-ANLC (Aungst, 2012). Eventually, interesting point was observed in ASM (i.n.) whereas asenapine blood and brain bioavailability was found to be 59.02% and 103.31%, respectively. These data indicated that apart from the advantages of nanocarriers in brain targeting, nasal route of delivery system is also contributing in brain delivery. This was directly evident by nearly equal brain availability and lower systemic availability of ASM by intranasal route in comparison to intravenous route. Overall, GC-ANLC demonstrated superior over the ANLC comparing drug targeting potential, brain availability and sustainability of drug.

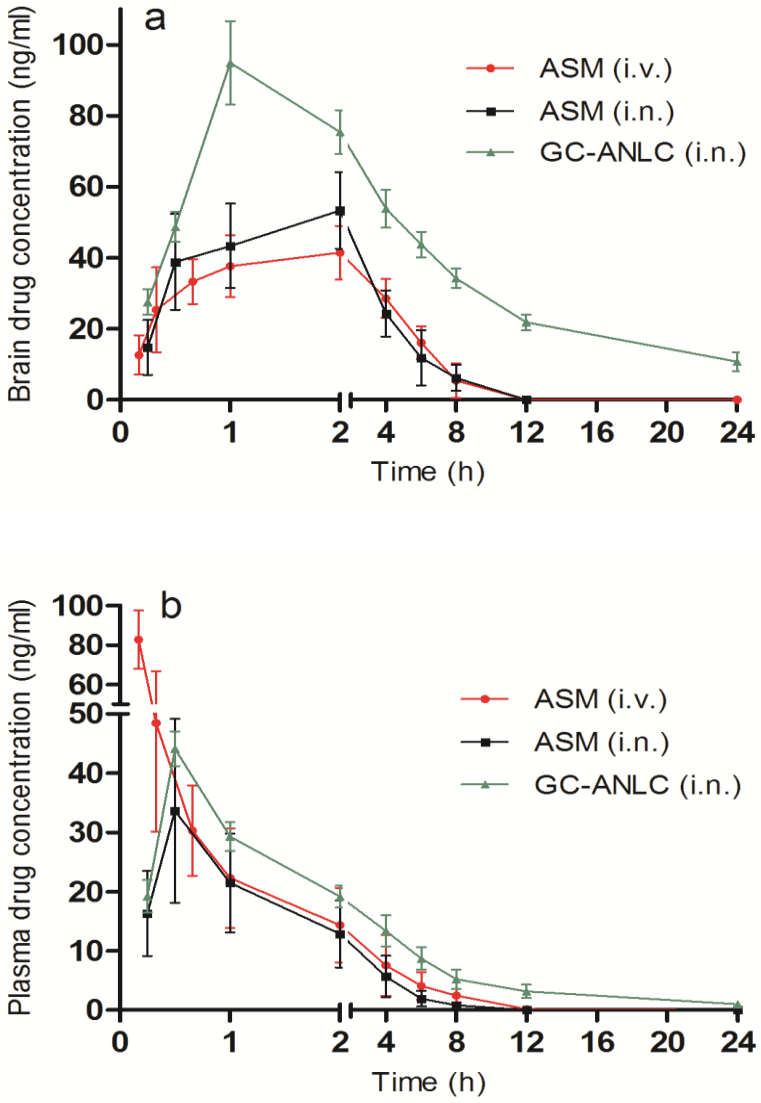

Figure 5.27: *In-vivo* brain uptake and pharmacokinetic study. Plasma (a) and brain (b) drug concentration time profile of ASM (via i.v. and i.n.) and GC-ANLC (via i.n.) route. mean±SD, n=5.

5.10. Animal behavioural studies

5.10.1. Induced locomotor activity test

The results of the locomotors activity test of ANLC and GC-ANLC compared to ASM are shown in Figure 5.28 and Figure 5.29, respectively. In the statistical analysis of ANLC group, two way ANOVA demonstrated a significant difference among group [F (3, 64) = 1287, $p<0.05$]. Moreover, there were no significant difference among days [F (3, 64) = 0.9212, $p>0.05$] and no significant interaction between group and days [F (9, 64) = 0.7116, $p>0.05$]. The post hoc test revealed a significant increase in locomotor count in control group as compared to vehicle control and reduction of locomotors count in ASM and ANLC group as compared to positive control during three week period of behavioural observation. Also significant difference in count were observed between groups treated with ASM and ANLC from day 1 to day 21 ($p<0.05$).

Further, in statistical analysis of the GC-ANLC group, two way ANOVA demonstrated a significant difference among group [F (3, 64) = 1424, $p<0.05$]. Moreover, there were no significant difference among days [F (3, 64) = 0.8649, $p>0.05$] and no significant interaction between group and days [F (9, 64) = 0.7528, $p>0.05$]. The post hoc test revealed a significant increase in locomotor count in control group as compared to vehicle control and reduction of locomotors count in ASM and GC-ANLC group as compared to positive control during three week period of behavioural observation. Also significant difference in count were observed between groups treated with ASM and GC-ANLC from day 1 to day 21 ($p<0.05$).

As shown in results of ANLC and GC-ANLC, it was postulate that the antagonistic activity was achieved by ASM, ANLC and GC-ANLC, demonstrated the sensitivity of asenapine against D2 receptor. Further, significant count reduction in GC-ANLC and ANLC as compared to ASM at same dose confirmed that nanostructure lipid carriers had ability to cross the blood brain barrier resulting in higher dose dependent D2 receptor antagonistic activity (Tarazi FI and Neill JC, 2013).

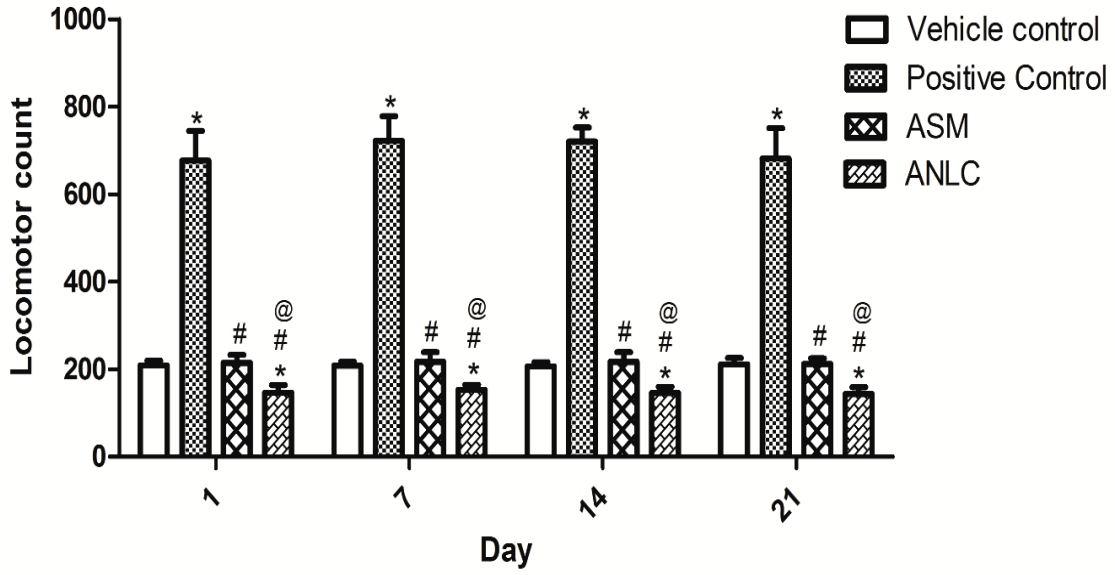

Figure 5.28: Locomotor activity response of vehicle control, positive control, ASM and ANLC groups on 1st, 7th, 14th and 21st day of study. * (p<0.05) compared to vehicle control; # (p<0.05) compared to positive control; @ (p<0.05) compared to ASM. The statistical calculation was performed by two way ANOVA followed by Bonferroni post-hoc test. mean±SD, n=5.

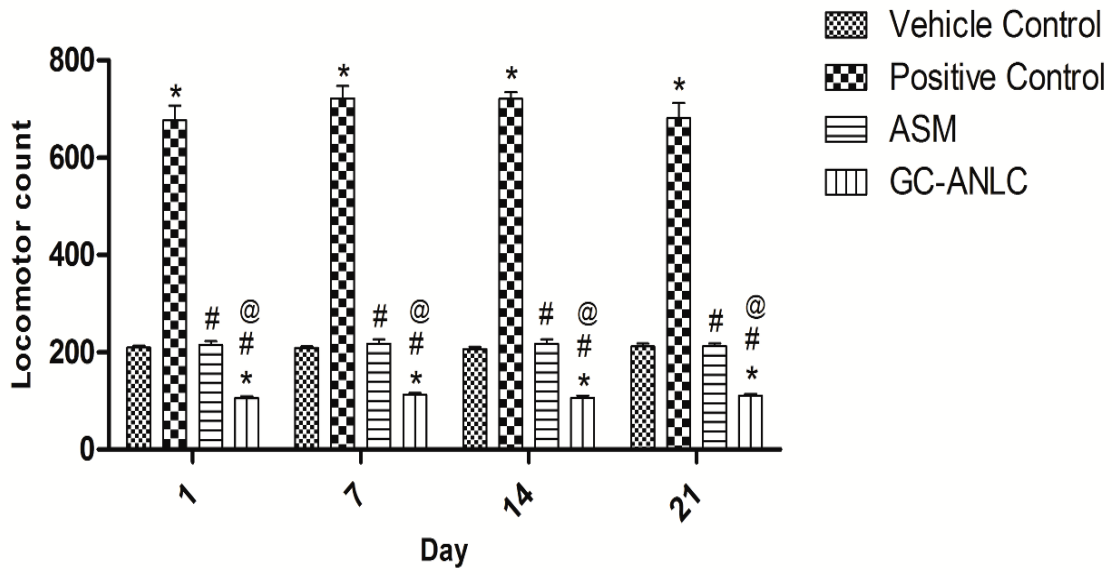

Figure 5.29: Locomotor activity response of vehicle control, positive control, ASM and GC-ANLC groups on 1st, 7th, 14th and 21st day of study. * (p<0.05) compared to vehicle control; # (p<0.05) compared to control; @ (p<0.05) compared to ASM. The statistical calculation was performed by two way ANOVA followed by Bonferroni post-hoc test. mean±SD, n=5.

5.10.2. Paw test

The FRT was defined as the time it took the rat to withdraw one forelimb from front hole. Likewise, the HRT was defined as the time it took the rat to withdraw one hindlimb from rear hole. One hour after drug administration, the four paws of each animal were placed in the holes on the surface of paw test platform. The paw test results of ANLC and GC-ANLC compared to ASM are shown in Figure 5.30 and Figure 5.31, respectively. In statistical calculation of paw test of ANLC group compared to vehicle control and ASM, the two way ANOVA of FRT showed significant difference among groups [F (2, 48) = 126.3, p<0.05]. However, there were no significant difference among days [F (3, 48) = 0.2879, p>0.05]. The interaction between group and days [F (6, 48) = 0.7424, p>0.05] were also not significant. The post-hoc analysis indicates significant increase in FRT in ASM and ANLC group when compared to vehicle control (p<0.05). However, no significant difference was found between ASM and ANLC on different day (p>0.05). The two way ANOVA of HRT demonstrated significant difference in groups [F (2, 48) = 1500, p<0.05] and days [F (3, 48) = 22.73, p<0.05]. Also, there was a significant interaction between the group and day [F (6, 48) =7.373, p<0.05]. Post-hoc analysis of HRT showed that ASM had significant difference in HRT on 7th, 14th and 21st day compared to 1st day (p<0.05), however, differences were not observed among 7th, 14th and 21st day (p>0.05). Inter-day analysis of ANLC demonstrated that there was no significant difference between 1st & 7th day (p>0.05) and 14th & 21st day (p>0.05) in HRT. Moreover, HRT of ANLC

formulation on 14th & 21st day response were significantly differ to 1st & 7th day (p<0.05) response.

Similarly, in statistical calculation of paw test of GC-ANLC group compared to vehicle control and ASM, the two way ANOVA of FRT showed that significant difference among groups [F (2, 48) = 113.1, p<0.05]. However, there were no significant difference among days [F (3, 48) = 0.4872, p>0.05]. The interaction between group and days [F (6, 48) = 0.6542, p>0.05] were also not significant. The post-hoc analysis indicates significant increase in FRT in ASM and GC-ANLC group when compared to vehicle control (p<0.05). However, no significant difference was found between ASM and GC-ANLC on different day (p>0.05). The two way ANOVA of HRT demonstrated significant difference in groups [F (2, 48) = 1100, p<0.05] and days [F (3, 48) = 14.01, p<0.05]. Also, there was a significant interaction between the group and day [F (6, 48) =4.347, p<0.05]. Post-hoc analysis of HRT showed that ASM had significant difference in HRT on 7th, 14th and 21st day compared to 1st day (p<0.05), however, differences were not observed among 7th, 14th and 21st day (p>0.05). Inter-day analysis of GC-ANLC demonstrated that there was no significant difference between 1st & 7th day (p>0.05) and 14th & 21st day (p>0.05) in HRT. Moreover, HRT of both 14th & 21st day were significantly differ to 1st & 7th day (p<0.05) in GC-ANLC.

ASM, ANLC and GC-ANC showed HRT greater than corresponding FRT. The significantly higher HRT right from 1st week in case of group treated with ANLC and GC-ANLC in comparison to corresponding groups treated with ASM indicates that

nanoformulation is better therapeutically. Higher HRT can be correlated to the increased asenapine concentration in brain owing to nanostructure lipid carrier delivery. It shows that developed nanostructure lipid carriers have potential to target brain resulting in higher HRT in ANLC and GC-ANLC group. It was also observed that HRT increased on subsequent days in groups treated with ASM, ANLC and GC-ANLC upto 1 and 2 week, respectively. This could be explained on the basis of pharmacological effect of asenapine which takes around 2 weeks to show optimum clinical benefit. The sustained and targeted delivery of asenapine by ANLC and GC-ANLC can be directly correlated to increase in HRT as compared to ASM during behavioural observation period.

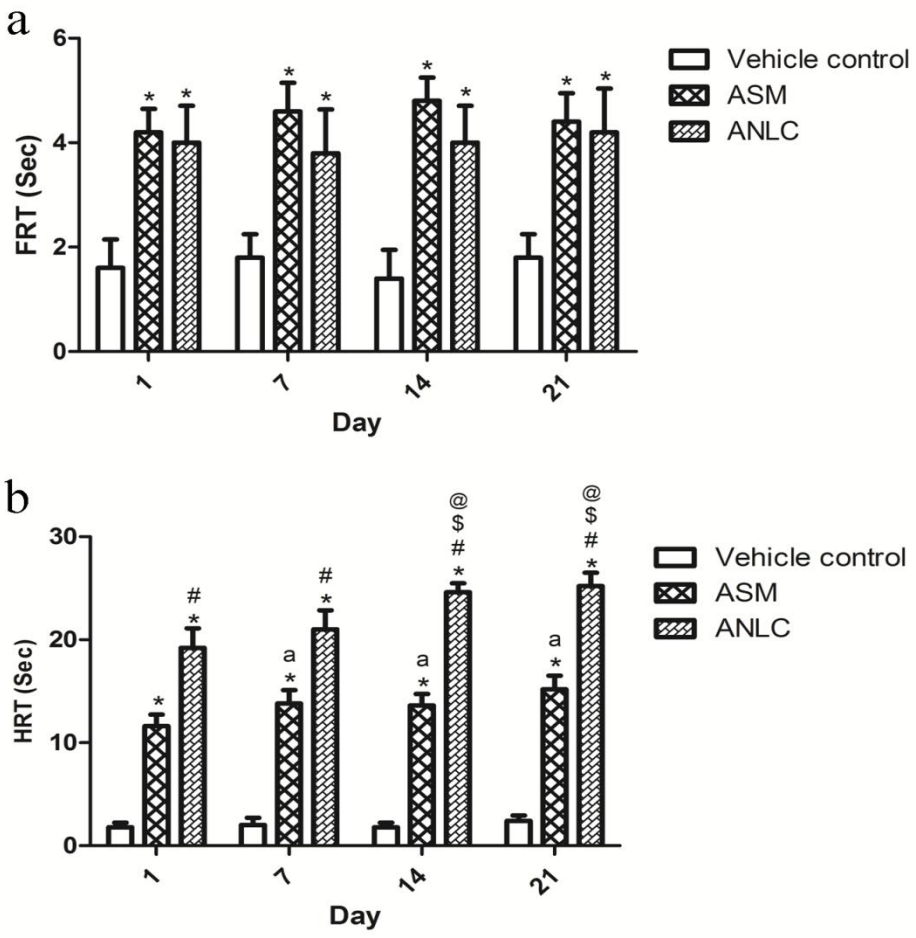

Figure 5.30: Paw test assessment of vehicle control, ASM and ANLC groups on 1st, 7th, 14th and 21st day of study. (a) Fore limb retraction time (FRT), * (p<0.05) compared to vehicle control (b) Hind limb retraction time (HRT), * (p<0.05) compared to vehicle control, # (p<0.05) compared to ASM, a (p<0.05) compared to 1st day response of ASM; $, @ ($p$<0.05) compared to 1st and 7th day response of ANLC, respectively. The statistical calculation was performed by two way ANOVA followed by Bonferroni post-hoc test. mean±SD, n=5.

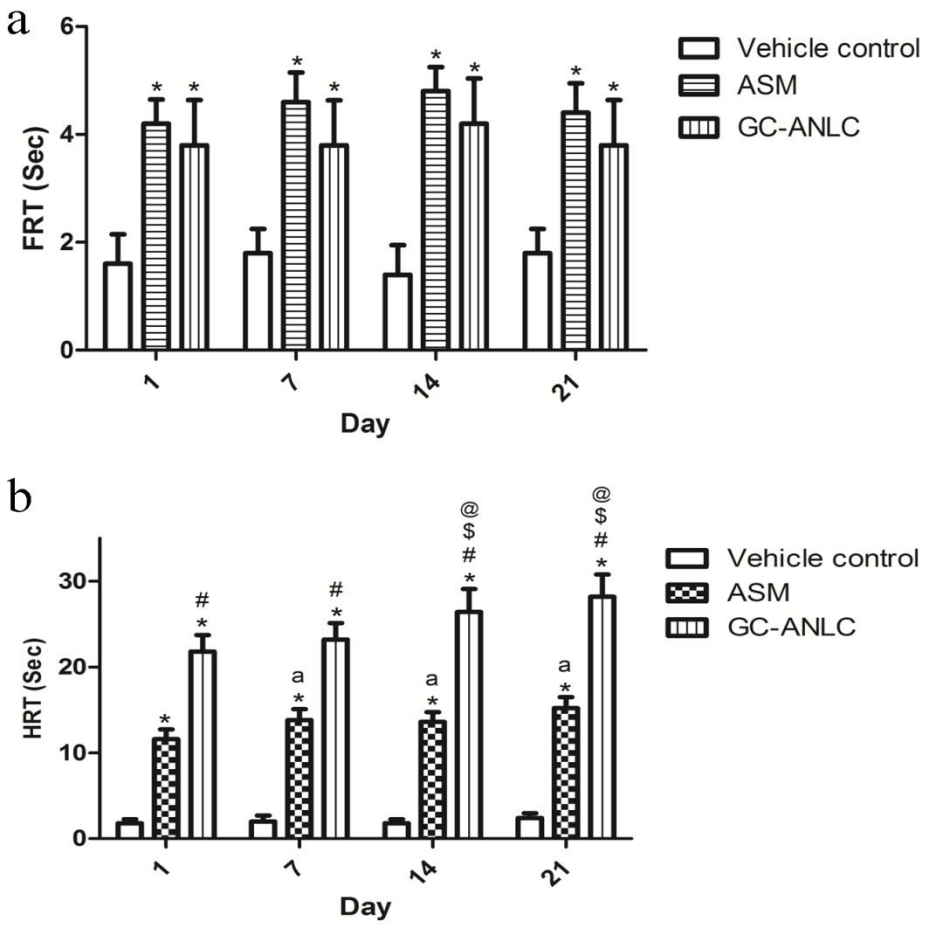

Figure 5.31: Paw test assessment of vehicle control, ASM and GC-ANLC groups on 1st, 7th, 14th and 21st day of study. (a) Forelimb retraction time (FRT), * (p<0.05) compared to vehicle control (b) Hindlimb retraction time (HRT), * (p<0.05) compared to vehicle control, # (p<0.05) compared to ASM, a (p<0.05) compared to 1st day response of ASM; $, @ ($p$<0.05) compared to 1st and 7th day response of GC-ANLC, respectively. The statistical calculation was performed by two way ANOVA followed by Bonferroni post-hoc test. mean±SD, n=5.

5.10.3. Catalepsy test

The cataleptic study was evaluated upto 21 day to observe effect of formulation on side effect associated with asenapine. Figure 5.32 and Figure 5.33 depict extrapyramidal side effect of ANLC and GC-ANLC compared to ASM in normal rats in terms of cataleptic behaviour. In statistical analysis of ASM and ANLC, two-way ANOVA revealed that there were significant difference among groups [F (2, 48) = 3152, $p<0.05$]. However, there were no significant difference among days [F (3, 48) = 1.087, $p>0.05$]. But, there was a significant interaction between group and days [F (6, 48) = 26.23, $p<0.05$]. The post hoc test showed that cataleptic response (Time in second) of ASM and ANLC differed significantly from control group ($p<0.05$) on all days. The first day observation showed no significant difference ($p>0.05$) in response between ASM and ANLC. However, responses exhibited on 7th ($p<0.05$), 14th ($p<0.05$) and 21st ($p<0.05$) day between ASM and ANLC groups were significant. When groups were compared on different days, catalepsis was significantly increased in ASM ($p<0.05$) and decreased in ANLC ($p<0.05$) on 7th, 14th and 21th day in comparison to response of 1st day. In both ASM and ANLC group, no significant difference ($p>0.05$) in inter day response amongst groups were observed between 14th and 21th day.

Similarly, the statistical analysis of ASM and GC-ANLC, two-way ANOVA revealed that there were significant difference among groups [F (2, 48) = 2849, $p<0.05$]. However, there were no significant difference among days [F (3, 48) = 0.9208, $p>0.05$]. But, there was a significant interaction between group and days [F (6, 48) =

23.10, $p<0.05$]. The post hoc test showed that cataleptic response of ASM and GC-ANLC were significantly different from control group ($p<0.05$) on all days. The first day observation showed no significant difference ($p>0.05$) in response between ASM and GC-ANLC. However, response exhibited on 7^{th} ($p<0.05$), 14^{th} ($p<0.05$) and 21^{st} ($p<0.05$) days of observation between ASM and ANLC group were significant. When groups were compared on different days, catalepsis was significantly increased in ASM ($p<0.05$) and decreased in ANLC ($p<0.05$) on 7^{th}, 14^{th} and 21^{th} day in comparison to response of 1^{st} day. In contrary to ANLC group, GC-ANLC group showed significant reduction ($p<0.05$) in interday response amongst groups observed between 14^{th} and 21^{th} day.

The reduction in cataleptic response by ANLC and GC-ANLC can be explained on the basis of sustained drug release, which leads to lesser fluctuation in drug concentration contributing clinical benefits in terms of constant antipsychotic efficacy and reduction of extra-pyramidal side effects. This could justify the superiority of sustained release over immediate release formulation for management of side effect in Schizophrenia (Baldwin CM and Scott LJ, 2009).

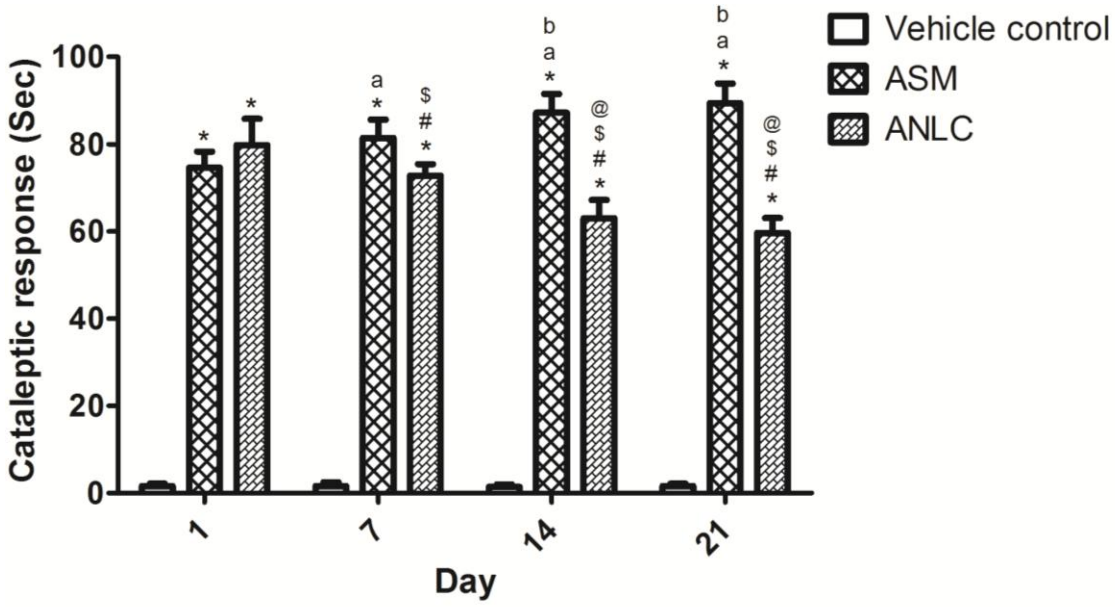

Figure 5.32: Animal cataleptic response of vehicle control, ASM and ANLC groups on 1st, 7th, 14th and 21st day of study. * (p<0.05) compared to vehicle control; # (p<0.05) compared to ASM; a, b (p<0.05) compared to 1st, 7th day response of ASM, respectively; $, @ ($p$<0.05) compared to 1st, 7th day response of ANLC, respectively. The statistical calculation was performed by two way ANOVA followed by Bonferroni post-hoc test. Mean±SD, n=5.

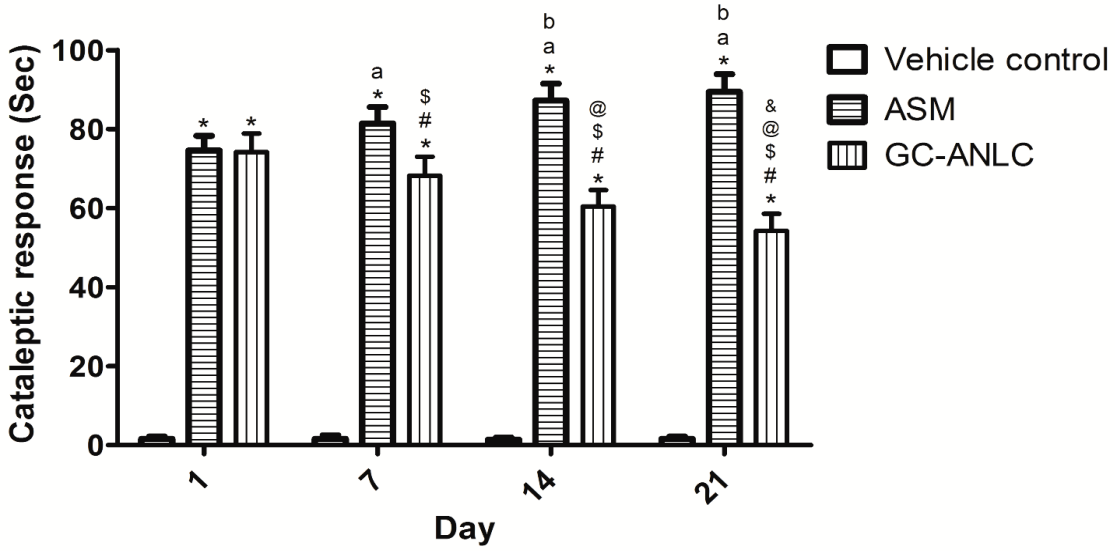

Figure 5.33: Animal cataleptic response of vehicle control, ASM and GC-ANLC groups on 1st, 7th, 14th and 21st day of study. * (p<0.05) compared to vehicle control; # (p<0.05) compared to ASM; a, b (p<0.05) compared to 1st, 7th day response of ASM, respectively; $, @ and & ($p$<0.05) compared to 1st, 7th and 14th day response of GC-ANLC, respectively. The statistical calculation was performed by two way ANOVA followed by Bonferroni post-hoc test. Mean±SD, n=5.

5.11. Toxicity studies

5.11.1. Nasal toxicity study

For any delivery system, the formulation should be compatible and tolerable at site of administration in long term use. The nasal mucosa is a very delicate tissue. So it was mandatory to check the GC-ANLC local toxicity and compatibility at nasal mucosa. Therefore, local toxicity of the GC-ANLC was evaluated on rat nasal mucosa relative to physiological saline (negative control) and isopropyl alcohol (positive control). The light photomicrographs of the rat nasal mucosa are shown in Figure 5.34. As shown in Figure 5.34 (a) and Figure 5.34 (c), GC-ANLC exhibited intact epithelial layer similar to nasal mucosa treated with physiological saline. The nasal mucosa treated with isopropyl alcohol showed major destruction of nasal epithelium membrane and damage underlying dermal connective tissue layer (Figure 5.34 (b)). This data suggested that GC-ANLC is biocompatible with nasal mucosa and seems to be safe for intranasal administration.

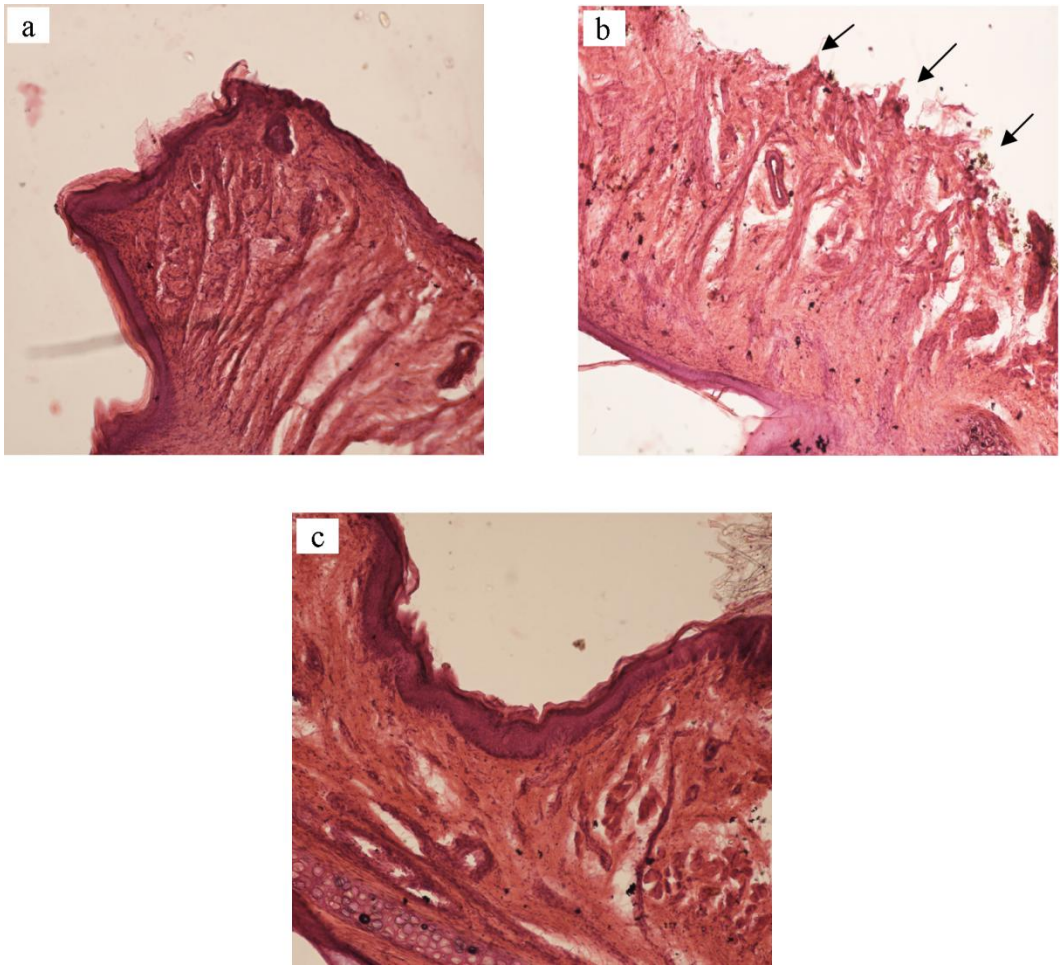

Figure 5.34: The light microscope photographs illustrate the histopathological condition of nasal mucosa (a) negative control rats treated with phosphate buffer (pH 6.4) showing intact mucosal epithelium, (b) positive control rats treated with isopropyl alcohol showing major destruction of nasal epithelium membrane (arrowhead), (c) GC-ANLC treated rats showing intact nasal mucosa without any histopathology damage.

5.11.2. Embryo fetal toxicity study

In this study, limited number of sporadic incidences of minor congenital malformations was observed in ASM exposed rat fetuses in comparison to GC-ANLC treated fetuses (Figure 5.35 and Figure 5.36). The percentage of fetal birth defects was found substantially deficient in GC-ANLC exposed group when compared to pure ASM administered group (Table 5.12). In the vehicle of ASM or blank nanosuspention treated groups, birth defects were detected almost negligible. Furthermore, one way ANOVA followed by Tukey's multiple comparison test indicate that there was substantial decrease in total number of the live fetuses and litter size ($F= (3, 12)\ 204.00$, $p<0.05$) in ASM exposed group only. Overall, exposure of GC-ANLC was found to be safer than ASM in relevance to developmental birth defects and litter size in rat fetuses.

The present study revealed that prenatal administration to GC-ANLC during the critical period of organogenesis (GD 6-21), induced limited number of minor birth defects as developmental embryo-fetotoxicity whereas these ailments were more pronounced in ASM treated embryo-fetuses, thus elucidates the better safety concern of asenapine nanostructured lipid carriers for teratogenic safety point of view. Our results were in consonance with the literature available on product monograph of the ASM that this drug may be teratogenic if used during early pregnancy. There is severe scarcity of literature on clinical and preclinical studies on this issue for valid comparison. Although several basic (exposure period, drug doses, route of administration, strain susceptibility, placental impairment) and

cellular/molecular (oxidative stress, antioxidant defense, apoptosis, protein synthesis, cytokines, growth factors, mitochondrial dysfunctions, default cell division, DNA/ RNA strand breaks) mechanisms of potential teratogenicity have been postulated so far to assess the causes of birth defects if any xenobiotic agent is insulted during highly sensitive phase of embryogenesis/ embryo-fetal development, since every developing organ has its vulnerable period (Holmes LB, 2002; Knudsen TB *et al.*, 2011; Pal Singh K and Tripathi N, 2015; Pauli RM *et al.*, 1987; Shum L *et al.*, 2003; Zeller R, 2010). During this period, genetically programmed cells are under the way of differentiation, migration and formation of different organs. The normal cellular processes could be disrupted by altering gene expression or interfering with signaling pathways in presence of toxic substance which may lead to emergence of vivid ailments in developing fetus/newborn, as found in our study. In the present experimental regimes, ASM and GC-ANLC were administered from 6 day to 21 day of gestation (the period of organogenesis with higher vulnerability), but only ASM could induce teratogenic effects in fetuses at 1.0 mg/kg dose whereas GC-ANLC could not induce similar effects, despite being equal in dose. Therefore, nanoformulations of novel antipsychotic drug, ASM; and possibly the other antipsychotic drugs could be a better and safe (teratogenic) option for drug delivery by nasal route in the pregnant women suffering with psychiatric disorders like schizophrenia.

Table 5.12: Effects of *in utero* exposure to ASM and GC-ASLC on congenital birth defects/ embryo-fetal development

SN	Malformations	Vehicle (water)(i.n.)	ASM (i.n.)	Blank Nanosuspension (i.n.)	GC-ANLC (i.n.)
1.	**Hemorrhages** (head & body)	00	03	02	03
2.	**Forelimbs**				
	Limb hyperflexion	00	13	01	07
	Malrotated limb	00	08	00	00
3.	**Hind limbs**				
	Malrotated limb	00	00	00	01
4.	**Fluid filled abdomen**	00	16	00	02
5.	**Eyes**				
	Ocular coloboma	00	08	00	00
6.	**Live fetus (total)**	37	20	33	34
7.	**Litter size**	09.25*±0.85	05.00±1.08	08.25*±1.43	08.50*±0.86

n=4 per group. Litter size represents Mean ± SEM value in all groups. * indicates significant difference (P<0.05) compared ASM (i.n.), one way ANOVA followed by Tukey's post hoc test.

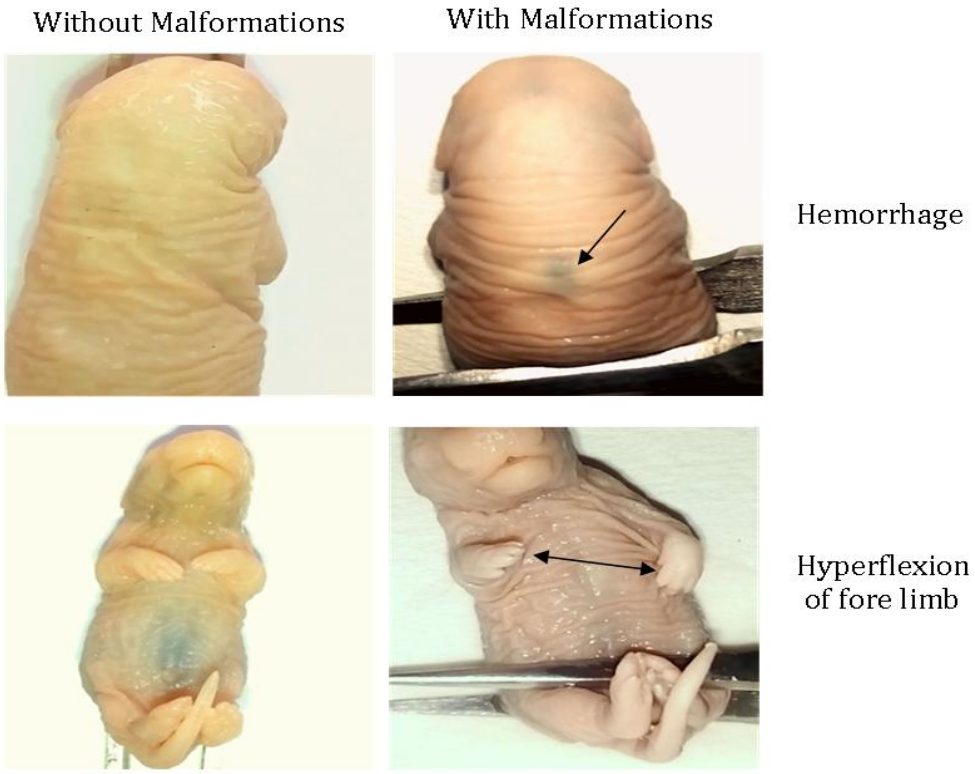

Figure 5.35: Representative photographs obtained from group treated with vehicle, i.n. (without malformation) and group treated with ASM, i.n. (with malformation- hemorrhage and hyperflexion of fore limb)

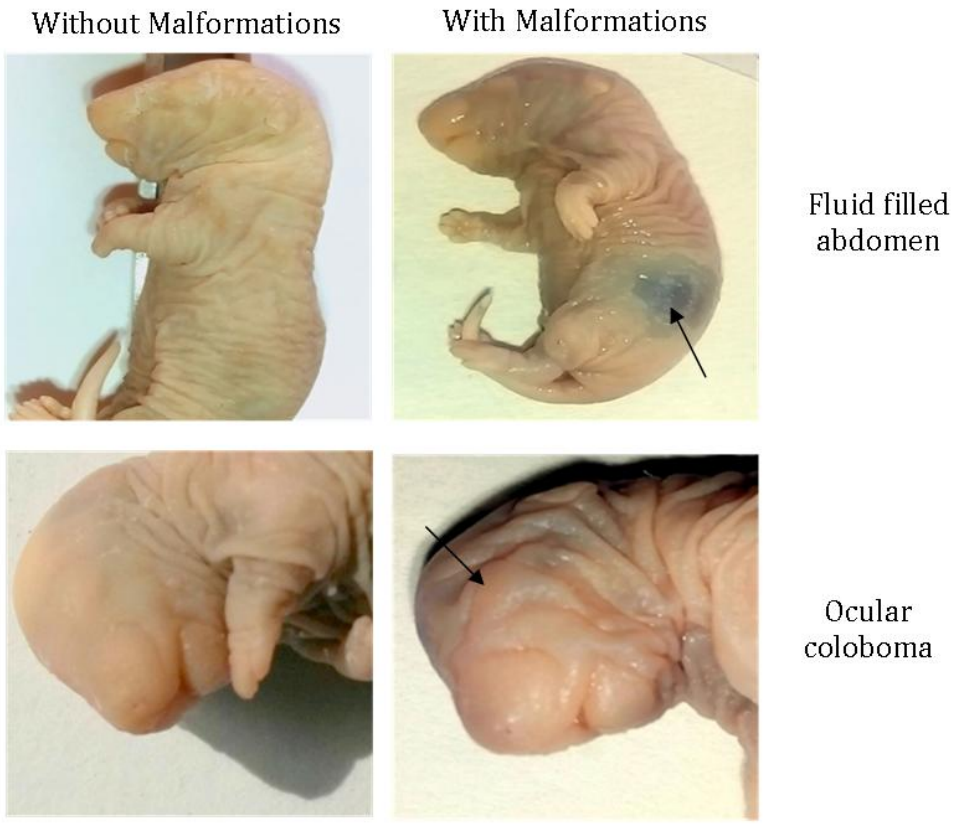

Figure 5.36: Representative photographs obtained from group treated with vehicle, i.n. (without malformation) and group treated with ASM, i.n. (with malformation- fluid filled abdomen and ocular coloboma)